HHS Public Access

Author manuscript

Cell. Author manuscript; available in PMC 2024 June 08.

Published in final edited form as:

Cell. 2023 June 08; 186(12): 2574–2592.e20. doi:10.1016/j.cell.2023.04.023.

Dissecting the Functional Organization of the *C. elegans* Serotonergic System at Whole-Brain Scale

Ugur Dag[1,4], **Ijeoma Nwabudike**[1,4], **Di Kang**[1,4], **Matthew A. Gomes**[1], **Jungsoo Kim**[1], **Adam A. Atanas**[1,2], **Eric Bueno**[1], **Cassi Estrem**[1], **Sarah Pugliese**[1], **Ziyu Wang**[1], **Emma Towlson**[3], **Steven W. Flavell**[1,5,*]

[1]Picower Institute for Learning & Memory, Department of Brain & Cognitive Sciences, Massachusetts Institute of Technology, Cambridge, MA, USA

[2]Computational and Systems Biology Program, Massachusetts Institute of Technology, Cambridge, MA, USA

[3]Department of Computer Science, Department of Physics and Astronomy, Hotchkiss Brain Institute, Alberta Children's Research Hospital, University of Calgary, Calgary, Alberta, Canada

[4]These authors contributed equally to this work.

[5]Lead Contact

SUMMARY

Serotonin influences many aspects of animal behavior. But how serotonin acts on its diverse receptors across the brain to modulate global activity and behavior is unknown. Here, we examine how serotonin release in *C. elegans* alters brain-wide activity to induce foraging behaviors, like slow locomotion and increased feeding. Comprehensive genetic analyses identify three core serotonin receptors (MOD-1, SER-4, and LGC-50) that induce slow locomotion upon serotonin release and others (SER-1, SER-5, and SER-7) that interact with them to modulate this behavior. SER-4 induces behavioral responses to sudden increases in serotonin release, whereas MOD-1 induces responses to persistent release. Whole-brain imaging reveals widespread serotonin-associated brain dynamics, spanning many behavioral networks. We map all sites of serotonin receptor expression in the connectome, which, together with synaptic connectivity, helps predict which neurons show serotonin-associated activity. These results reveal how serotonin acts at defined sites across a connectome to modulate brain-wide activity and behavior.

*Correspondence: flavell@mit.edu.

AUTHOR CONTRIBUTIONS

Conceptualization, U.D., I.N., D.K, and S.W.F. Methodology, U.D., I.N., D.K, J.K., A.A.A, E.B., S.P., Z.W., E.T., and S.W.F. Software, I.N., D.K., J.K., A.A.A., E.B., S.P., E.T., and S.W.F. Formal analysis, U.D., I.N., D.K., and S.W.F. Investigation, U.D., I.N., D.K., M.A.G., J.K., C.E. Writing – Original Draft, U.D., I.N., S.W.F Writing – Review & Editing, U.D., I.N., D.K., and S.W.F. Funding Acquisition, E.T. and S.W.F.

DECLARATION OF INTERESTS

The authors declare no competing interests.

ETOC

Comprehensive genetic analysis of serotonin receptors and brain-wide imaging in freely moving *C. elegans* provide a global view of how serotonin acts on specific receptors at defined sites in a connectome to modulate brain-wide activity and behavior.

Graphical Abstract

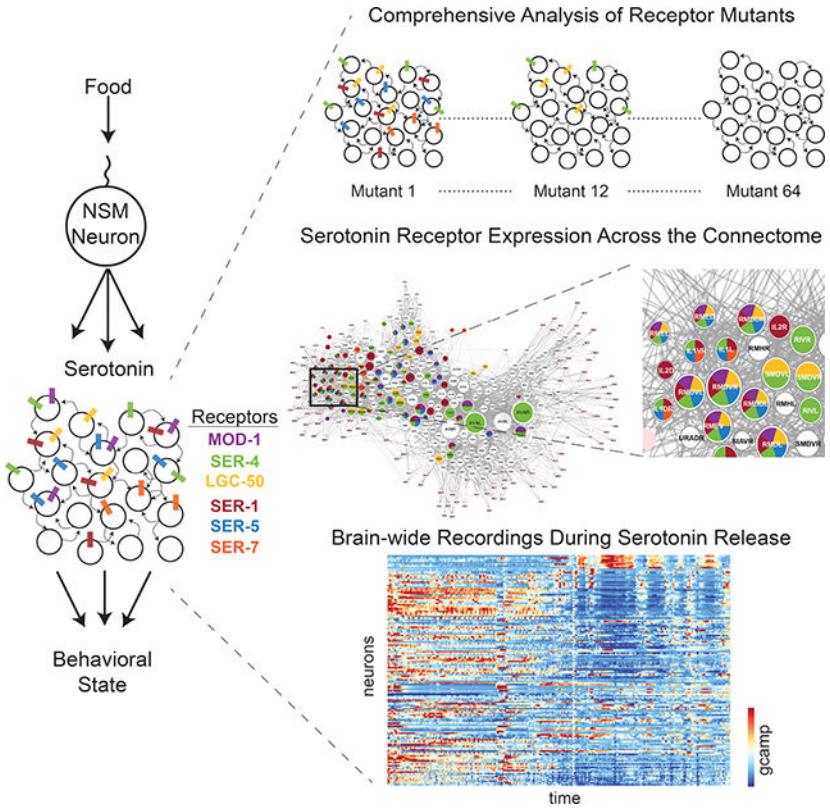

INTRODUCTION

Serotonin signaling is involved in many aspects of behavior and cognition, and dysfunction of the serotonergic system is implicated in psychiatric disease[1,2]. It is the most common target of psychiatric drugs, and many psychotropic chemicals like psilocybin and LSD act on serotonin receptors[3–5]. Efforts to understand how serotonin influences behavior have been hindered by its complexity. The neurons that release serotonin are functionally diverse, project broadly throughout the brain, and exert their effects via 14 different receptors[6,7]. Developing an integrative framework for serotonergic function that relates anatomy, receptors, circuits, and behavior across a whole nervous system would greatly aid our understanding of this important neuromodulatory system.

In mammals, serotonin is released by many subtypes of serotonergic neurons in the Raphe nuclei, each with distinct widespread projections to distal brain regions[8–11]. Recordings from this heterogeneous population have revealed diverse activity profiles, reflecting rewarding stimuli like food and complex cognitive processes[12–16]. This likely reflects

the diverse inputs onto these neurons[17]. The outputs of the serotonergic neurons are also complex: optogenetic stimulation of serotonergic neurons in rodents can elicit many behavioral effects, including slow locomotion, waiting/perseverance, and changes in reward learning[10,13,18–20]. In humans, alterations in serotonin levels modulate related behaviors, such as impulsivity and decision-making[21–23]. Serotonin acts through many distinct receptor types[2,6] and different cell types in a microcircuit typically express distinct serotonin receptors[24,25]. Cellular recordings have shown bulk effects of serotonin application on individual cell types[26,27]. However, these studies do not necessarily predict in vivo changes in activity during serotonin release[28]. In humans, changes in functional connectivity between areas with different serotonin receptor expression patterns are associated with stereotyped behavioral changes[29], suggesting important links between receptor expression, neural dynamics, and behavior. However, it has been challenging to develop a mechanistic understanding of how dynamic serotonin release in live animals engages specific serotonin receptors to alter neural dynamics and behavior.

It should be feasible to address these complexities in the nematode *C. elegans*, whose nervous system has 302 identifiable neurons with known connectivity[30–32]. The serotonergic system is important for *C. elegans* behavior and its organization resembles that of mammals. *C. elegans* utilizes the same synthesis (*tph-1*/TPH, *bas-1*/AAAD), vesicle loading (*cat-1*/VMAT), and reuptake (*mod-5*/SERT) machinery. It also has many of the same receptor types[33]. The few-to-many anatomical organization of the serotonergic system is also preserved in *C. elegans*: there are three pairs of serotonergic neurons (NSM, HSN, and ADF) while >100 neurons are estimated to express serotonin receptors[33,34].

When *C. elegans* eat appetitive bacterial food, they display adaptive behavioral changes that are controlled by serotonin: slow locomotion, increased feeding, and increased egg-laying[35–39,39,40]. While egg-laying is controlled by the serotonergic neuron HSN in the midbody, the other food-induced behavioral changes are controlled by the serotonergic neuron NSM in the head[35–38]. NSM extends a sensory dendrite into the pharyngeal lumen and directly senses bacterial food the animal is eating. NSM is only active while animals are eating bacteria[37] and its activity is strongly correlated with slow locomotion[35–37,41]. NSM appears to act through volume transmission: it releases serotonin at non-synaptic neurosecretory release sites adjacent to the nerve ring, the main *C. elegans* neuropil containing fibers from 196 neurons[31,42]. Six *C. elegans* serotonin receptors have been identified. Four of these have been suggested to influence locomotion (MOD-1, SER-1, SER-4, SER-5) and one influences feeding (SER-7)[33,43–45]. However, how these receptors are functionally organized to control behavior remains unknown. Given that these receptors are co-activated during volume transmission, how do they interact with one another? How is serotonin receptor expression arranged in the connectome? And how does serotonin binding to these diverse receptors across many cell types alter brain dynamics and behavior?

Here, we provide a global characterization of the serotonergic system that links these scales of analysis. Serotonin release by NSM alters locomotion in a manner that depends on all six serotonin receptors. We decipher the functional roles of the receptors, and the interactions between them, by examining serotonin-induced behavior in a panel of 64 mutant strains that lack all combinations of receptors. This analysis also reveals that the receptors support

different changes in behavior, with some receptors supporting a transient behavioral change in response to sudden increases in serotonin release and others supporting a persistent behavioral change during continued release. We layer these findings onto brain-wide activity changes during serotonin release, which we map onto the worm's physical wiring diagram. This reveals widespread NSM-associated brain dynamics that are partially predicted by the serotonin receptor expression profiles and synaptic connectivity of the neurons. These results provide a global view of how serotonin acts on specific receptors at defined sites in a connectome to modulate brain-wide activity and behavior.

RESULTS

An experimental platform to study serotonin-induced behavioral changes

When animals encounter and start eating bacteria, the serotonergic neuron NSM is activated, and its activity correlates with slow locomotion[36,37]. Previous studies showed that NSM inactivation or serotonin depletion (via *tph-1* mutation) attenuates this feeding-induced behavioral change but does not abolish it[36,37]. Thus, NSM serotonin strongly contributes to food-induced slowing, but other pathways also contribute. To obtain a system where serotonin acts on its own to alter neural activity and behavior, we optogenetically activated NSM with Chrimson in animals that were not consuming bacteria. This induced a decrease in locomotion speed and head movements and an increase in feeding (i.e. pharyngeal pumping), similar to when animals encounter food (Fig. 1A; Fig. S1A). These effects were abolished in *tph-1* mutants (Fig. 1A), indicating that they require serotonin release.

We considered which optogenetic stimulation patterns would best mimic endogenous NSM activity. While animals are feeding, NSM exhibits long phasic bouts of activity of varying amplitudes and durations (1min to >10min)[41]. To test whether the amplitudes of NSM activity bouts reflect salient environmental cues, we recorded NSM activity as animals encountered a bacterial food patch containing different densities of food arranged in concentric rings, with the densest food at the center (Fig. 1B–C). NSM activity increased upon initial food encounter and increased further when animals subsequently encountered the denser part of the food patch. Thus, amplitudes of NSM activity bouts reflect food density. NSM activity bouts continue for many minutes (Fig. 1B, right), during which time they are anti-correlated with animal speed. Previous work showed they eventually terminate in a manner that is closely aligned with the onset of roaming behavior[41].

We optogenetically activated NSM in the absence of food with different waveforms of light to mimic NSM activity bouts of different amplitudes and durations, matching our NSM recordings[37]. Control experiments with simultaneous NSM calcium imaging confirmed that these different optogenetic stimuli induced expected changes in NSM activity (Fig. S1B). Wild-type animals exhibited behavioral responses that tracked the optogenetic stimulus: the magnitude of the speed reduction scaled with stimulus intensity, and its duration scaled with the stimulus duration (Fig. 1E). Behavioral responses were abolished in serotonin-deficient *tph-1* mutants and in sextuple mutants lacking all six known *C. elegans* serotonin receptors (*ser-1, ser-4, ser-5, ser-7, mod-1,* and *lgc-50*; Fig. 1D–E). Thus, this paradigm allows us to evoke serotonin release and examine how activation of defined serotonin receptors modulates circuit activity to drive the behavioral response.

Six *C. elegans* serotonin receptors interact to control locomotion

We next examined how each serotonin receptor contributes to the NSM-induced behavioral change. First, we crossed NSM::Chrimson into the six single mutants lacking individual serotonin receptors. The behavioral response of each mutant was attenuated compared to wild type, though none had abolished slowing (Fig. 2A–C; shown as speed normalized to pre-stimulus baseline speeds, which were similar to wild type, Fig. 2B). This indicates that each receptor plays some role in NSM-induced slowing. We next crossed NSM::Chrimson into the quintuple mutant strains that have only one serotonin receptor remaining (referred to as *mod-1*-only, etc, though we note that there could be unidentified receptors). Mutants with only *mod-1, ser-4,* or *lgc-50* intact displayed NSM-induced slowing, though to varying degrees (Fig. 2A–C). Mutants with only *ser-5* and *ser-1* intact displayed almost no slowing, and mutants with only *ser-7* intact did not slow at all. These data already suggested potential complexities in how the serotonin receptors interact to control slowing. For example, the loss of *ser-1* caused a greater deficit in slowing than the loss of *ser-4*. However, *ser-4* on its own could promote robust slowing while *ser-1* could not (Fig. 2A–C).

To decipher how these receptors interact, we crossed NSM::Chrimson to 64 different mutant backgrounds that lacked all possible combinations of serotonin receptors and quantified their NSM-induced slowing. This analysis indicated that *mod-1, ser-4,* and *lgc-50* are the primary receptors that drive slowing, so we refer to them as the “driver” receptors. The triple mutant lacking these three receptors displayed a slowing deficit almost as severe as the sextuple mutant, while the double mutants lacking combinations of them had more mild phenotypes (Fig. 2D). In addition, as described above, the quintuple mutants with any of these three receptors intact displayed NSM-induced slowing (Fig. 2A–D). This indicates that concurrent activation of three serotonin receptors produces most of the slowing response observed in wild-type animals.

The other three receptors, *ser-1, ser-5,* and *ser-7,* had modulatory roles (referred to as the “modulator” receptors). They were not strictly required for slowing, since the triple mutant lacking all three had no deficit (Fig. 2E), and they could not promote robust slowing on their own (Fig. 2A–D). However, in many strains with different combinations of other serotonin receptors deleted, the loss of these receptors caused large deficits. Fig. 2F shows the effects of deleting each of these receptors in each genetic background (with different serotonin receptors already deleted). *ser-7* primarily inhibits slowing (Fig. 2F, orange bars are mostly negative), while *ser-1* and *ser-5* had mixed effects depending on the background. Deletion of these receptors had little to no effect if the drivers of slowing (*mod-1, ser-4, and lgc-50*) were already deleted (Fig. 2D), suggesting that they modulate slowing induced by the driver receptors. Overall, these results suggest that there is one subset of serotonin receptors (*mod-1, ser-4*, and *lgc-50*) that drive a change in locomotion and a second subset (*ser-1*, *ser-5*, and *ser-7*) that, when co-activated together with the driver receptors, modulate this behavior.

To discern the exact form of these receptor interactions, we constructed a model that predicts the amplitude of NSM-induced slowing across all genotypes based on which serotonin receptors were present (Fig. 2G). A linear model with six predictor terms, indicating the presence or absence of each receptor, only predicted slowing across the genotypes with

partial accuracy, even when trained on all genotypes (Fig. 2H; 72% variance explained). This indicates that slowing across the full set of genotypes cannot be fully described by a weighted sum of which receptors are present. Therefore, we added additional predictor terms to the model that described the joint presence of two or more receptors (for example, whether *mod-1* and *ser-4* are *both* present), allowing for receptor interactions. We only added interaction terms if they were necessary to explain a non-linearity in how two or more receptors interact (see Methods). 18 interaction terms were added, which significantly increased model performance (90% variance explained, Fig. 2I–J). When this model was trained on data lacking individual genotypes, it was able to predict the behavior of the withheld genotype, suggesting that receptor interactions are similar across genotypes (Fig. S2A). The interaction terms that improved model performance reflected genetic redundancies and antagonistic interactions between “driver” and “modulatory” receptors (Fig. S2B). These results suggest that extensive interactions between serotonin receptors shape their functional roles in modulating behavior.

Satiety modulates the functional roles of the serotonin receptors

An integral aspect of serotonergic signaling in *C. elegans* is its increased functional prominence in fasted animals. When *C. elegans* are fasted they display exaggerated food-induced slowing, referred to as enhanced slowing, an effect that requires NSM and serotonin[36–38]. Consistent with this literature, we found that fasted animals displayed more persistent reductions in speed upon NSM stimulation (Fig. 3A–B).

Fasting could enhance NSM-stimulated slowing by (i) increasing NSM-stimulated serotonin release, (ii) increasing serotonin receptor expression; (iii) enhancing how the receptors drive slowing due to changes in receptor-expressing cells (for example, stronger coupling of those cells to behavior), or (iv) altering how the receptors interact (for example, making receptors act more synergistically). To begin to distinguish among these possibilities, we examined whether slowing was enhanced by fasting in the quintuple mutants (Fig. 3A–B). NSM-stimulated slowing was enhanced by fasting in animals with *mod-1* or *lgc-50* intact, but not in animals with only *ser-4*. This renders it unlikely that there is increased serotonin release upon optogenetic NSM stimulation in fasted animals, as this would have been predicted to increase NSM-stimulated behavioral responses in *ser-4*-only mutants also. (NSM-induced slowing in well-fed *ser-4*-only animals is not saturated, Fig. S3A–B). The enhanced slowing also does not appear to be due to changes in the expression of those receptors. The neurons expressing these receptors do not change (see Fig. S5B) and we previously showed that overall mRNA translation levels for these genes do not change[46]. This suggests that fasting enhances how MOD-1 and LGC-50 receptor activation impacts neural circuit activity to drive slowing.

To examine whether fasting also alters the functional interactions between receptors, we recorded NSM-stimulated behavioral responses in well-fed and fasted conditions for all 64 serotonin receptor mutant strains. We asked whether the effect of deleting a given serotonin receptor in each genetic background (with some serotonin receptors already deleted) was altered by fasting (Fig. 3C). Using stringent statistical criteria (see Methods), we observed many significant differences between fed and fasted animals. For example,

whereas the function of *mod-1* was similar in both states, *ser-1* and *lgc-50* often had stronger contributions to slowing after fasting. In addition, there were examples of inversions of function, where loss of a receptor exaggerated slowing in well-fed animals, but attenuated slowing in fasted animals (e.g. *ser-5*). This suggest that interactions among the receptors are also modulated by satiety.

MOD-1 and SER-4 confer behavioral responses to different patterns of serotonin release

Different serotonin receptors exhibited striking differences in the behavioral dynamics that they support. This was immediately apparent in the quintuple mutants that have only one serotonin receptor intact (Fig. 4A–B). For the three receptors that "drive" slow locomotion, the maintenance of slow locomotion during continued NSM stimulation differed. *mod-1*-only mutants displayed reduced locomotion as long as NSM was active, but *ser-4*-only mutants only displayed a transient reduction in locomotion speed at stimulation onset. *lgc-50*-only animals displayed an intermediate response (Fig. 4A–B). Consistent with this, *mod-1*-only animals displayed longer durations of slowing during longer NSM stimuli, but *ser-4*-only animals did not (Fig. 4C–D). This suggests that *mod-1*-only animals exhibit behavior that tracks the continued release of serotonin, but *ser-4*-only animals do not. This difference could not be explained as an indirect consequence of different magnitudes of slowing, as it was consistent across NSM stimuli that evoked different levels of slowing. We asked whether these differences in the quintuple mutants generalized to other genotypes. Indeed, all genotypes with *mod-1* and *lgc-50* intact had sustained NSM-induced slowing, and all mutants lacking these two receptors did not (Fig. 4E). These data suggest that activation of different serotonin receptors drives different dynamical changes in behavior.

The difference between *mod-1* and *ser-4* was especially striking. To more closely examine this, we compared these strains' behavioral responses to other patterns of NSM activation. A stimulation pattern with an immediate activation of NSM::Chrimson further accentuated the difference: *ser-4*-only animals transiently slowed down upon NSM activation, while *mod-1*-only animals maintained slow locomotion (Fig. 4F). We also tested a stimulation pattern with a ramping onset that never contained a high positive derivative. *mod-1*-only animals slowed down in response to this pattern, but *ser-4*-only animals did not (Fig. 4G). To quantify these effects more precisely, we fit a model that predicts the slowing dynamics of these genotypes based on the dynamic NSM stimulus. The model parameters for *mod-1*-only animals indicated that they primarily weigh ongoing NSM stimulation levels, while the parameters for *ser-4*-only indicated that they primarily respond to the derivative of NSM stimulation (Fig. S4A).

To examine whether these findings generalize to natural bouts of NSM activation, we examined mutant animals' speed upon bacterial food patch encounter, which leads to immediate activation of NSM[36,37] (Fig. S4B). Food-induced slowing is partially dependent on serotonin, so animals lacking all six serotonin receptors displayed an attenuated speed reduction after food encounter, though (as described above) this only partly attenuates slowing (Fig. S4B). *mod-1*-only animals had wild-type slowing, matching the optogenetics results (Fig. 3A). *ser-4*-only animals displayed a rapid slowdown upon food encounter that exceeded the level in the sextuple mutants, but after one minute, their speed matched the

sextuple mutants, also providing a qualitative match to the optogenetics results. Together, these data suggest that *mod-1* confers sustained behavioral responses to sustained NSM activation, while *ser-4* confers responses to abrupt increases in NSM activation.

mod-1 is a serotonin-gated chloride channel (a $5HT_3$ homolog) and *ser-4* is a $G_{i/o}$-coupled G protein-coupled receptor (a $5HT_{1A}$ homolog). Both are known to act in an inhibitory fashion[47,48]. In principle, this difference between *mod-1* and *ser-4* could be due to differences in serotonin release dynamics (due to feedback to NSM), the molecular properties of the receptors, or the properties of the neurons where these inhibitory receptors are expressed. We first examined whether altered serotonin release dynamics could explain these effects. If serotonin release dynamics are different in these two mutants, then other NSM-induced behavioral changes should also show different dynamics. We tested this by examining NSM-induced feeding behavior in mutants with *mod-1* or *ser-4* present (along with *ser-7*, which is required for serotonin-induced feeding[49]). The difference in locomotion decay rates was still evident when comparing *mod-1/ser-7*-only to *ser-4/ser-7*-only animals (Fig. 4H). However, NSM-stimulated feeding behavior was the same in both strains (Fig. 4H; feeding behavior was not saturated). This suggests that it is unlikely that serotonin release is different between the two strains.

We next tested whether these differences between *mod-1* and *ser-4* were due to the different cell types in which they were expressed or, alternatively, their different molecular properties. Given that they are both inhibitory receptors, we tested this by swapping their sites of expression and examining the impact on NSM-induced behavior. Sextuple mutants expressing *mod-1* under the *ser-4* promoter (*Pser-4::mod-1*) displayed transient slowing upon serotonin release, matching *ser-4*-only mutants and the *Pser-4::ser-4* animals (Fig. 4I–J). In contrast, animals expressing *ser-4* under the *mod-1* promoter (*Pmod-1::ser-4*) displayed maintained slowing throughout the optogenetic stimulus, matching *mod-1*-only mutants and *Pmod-1::mod-1* animals (Fig. 4I–J). Thus, the functional roles of the receptors tracked the promoter used, rather than the molecular identity of the receptor being expressed. We note that the expression patterns of these promoters might only partially recapitulate the native expression patterns of these genes. Nevertheless, these results provide evidence that the sites of expression of these two receptors, rather than their molecular properties, play a dominant role in conferring the behavioral dynamics they support. The *ser-4*-expressing neurons are sensitive to sudden increases in NSM activity, while the *mod-1*-expressing neurons are sensitive to the overall level of NSM activity. Whether there is additional functional heterogeneity among the neurons that express each of these receptors is addressed below.

Mapping sites of serotonin receptor expression across the *C. elegans* connectome

The above results indicate that the expression patterns of the serotonin receptors are important in conferring their functional roles. Therefore, we next determined where each serotonin receptor was expressed across the connectome. We used CRISPR/Cas9 genome editing to insert T2A-mNeonGreen fluorescent reporters into each of the six serotonin receptor genes, just before their stop codons (Fig. 5A). Under this strategy, cytosolic

mNeonGreen in each of these six strains should be expressed in neurons that match the native pattern of each serotonin receptor's expression.

To determine the ground-truth identities of the fluorescent neurons labeled in each strain, we crossed the NeuroPAL transgene into each reporter strain (Fig. 5A; Fig. S5A). The NeuroPAL transgene expresses three fluorescent proteins (NLS-mTagBFP, NLS-CyOFP1, NLS-mNeptune2.5) under well-defined genetic drivers, so that neural identity can be inferred from position and multi-spectral fluorescence[50]. We annotated the identities of all mNeonGreen-positive neurons in 5–10 adult animals per strain (Fig. S5B). Expression was very similar for well-fed and fasted animals, with a few exceptions: *ser-4* in ADE and AIN, *ser-5* in AVE and IL1, and *lgc-50* in DVB and AUA (Fig. S5B). Each receptor was expressed in 9–24 of the 118 *C. elegans* neuron classes (Fig. 5B). Altogether, 52 neuron classes expressed at least one receptor (Fig. 5C). Our results were broadly in agreement with existing single-cell sequencing data[34], though there were some differences, potentially because the sequencing results are based on mRNA levels and our work here is based on protein levels.

While each serotonin receptor was expressed in a unique pattern, the level of overlap between the receptors was higher than the level expected by chance for most pairs (Fig. 5D). Some individual neuron classes express as many as five different serotonin receptors. We previously used an identical strategy to construct reporters for other GPCRs that showed completely different expression patterns[46], indicating that correlated expression among the serotonin receptors is not an artifact of the reporter strategy. This high incidence of serotonin receptor co-expression might underlie some of the functional interactions among the receptors.

The receptors were significantly enriched in interneurons, significantly de-enriched in motor neurons, and partially enriched in sensory neurons (Fig. 5E). The *C. elegans* nerve ring consists of four major strata, or interconnected groups of neurons[51,52]. Serotonin receptor expression was enriched in stratum 1, associated with head movements and exploration, and de-enriched in stratum 3, associated with aspects of movement control (Fig. S5C). *mod-1* and *ser-4* were also enriched in the "Rich Club" neurons, a group of interneurons that span the strata and influence locomotion[53] (Fig. S5D). *ser-7* was enriched in the pharyngeal nervous system (Fig. S5D), consistent with its role in feeding[49]. These analyses reveal broad and correlated expression of the serotonin receptors in circuits that control different aspects of behavior.

Different temporal phases of the MOD-1-induced behavioral change map onto different sites of expression

We next determined which sites of receptor expression are functionally important for locomotion. We chose to examine this for *mod-1*, since sole expression of *mod-1* can confer rapid and sustained changes in locomotion. We engineered a mutant allele of *mod-1* in which the orientation of several exons was inverted, inactivating the gene (Fig. 5F). These exons were flanked by dual lox sites that could re-invert the orientation of the exons upon Cre expression, which should restore gene function. This strategy constrains expression levels so that cell-specific expression of *mod-1* never exceeds native levels. This allele

was engineered into the *mod-1*-only quintuple mutant and the resulting strain displayed no serotonin-induced slowing, matching the sextuple mutant (Fig. 6B). This indicates that the *mod-1* exon inversion successfully inactivated *mod-1* (Fig. 6B). Pan-neural Cre expression led to a full rescue of the *mod-1*-only locomotion phenotype (Fig. 6B), indicating that Cre expression can successfully invert the *mod-1* gene in neurons and rescue *mod-1* function.

We next performed cell-specific rescues in the majority of the *mod-1*-expressing neurons using Cre drivers that drive expression in unique sets of these neurons. We identified three types of neurons. First, there were several neurons where *mod-1* genetic rescue did not restore slowing (RME, RIS, ADE, NSM, RIC, AIM, AIY, AIZ, AVE; Fig. S5E). Second, there were two neurons where *mod-1* genetic rescue caused animals to display a transient slowdown upon NSM activation, similar to *ser-4*-only animals (RID, ALA; Fig. 5G–I). Third, there was one neuron where *mod-1* rescue led to an unusual slow onset, sustained slowing upon NSM activation (RIF, Fig. 5G–I). Interestingly, we found that we could restore both the transient and sustained slowdown by combined genetic rescue in cells from both categories (ALA+RIF; Fig. 5G–I). This suggests that the initial slowdown upon NSM activation and the sustained slowdown during NSM activation are separable effects, mediated by *mod-1* function in different neurons. In addition, given the partial rescues observed for the rescuing Cre lines, *mod-1* likely functions in several neurons to promote slowing.

NSM activity is associated with widespread changes in neural activity across the brain

We next examined how NSM activity was associated with changes in neural activity across the brain. We performed brain-wide calcium imaging in seven freely-moving animals as they navigated to and encountered a food patch, a natural context where NSM is activated to modulate locomotion. We used a strain expressing NLS-GCaMP7f and NLS-mNeptune2.5 in all neurons (Fig. S6A). Animals were recorded on a previously-described live-tracking microscope with two light paths[54]. A spinning disc confocal below the animal allows for fast volumetric imaging of fluorescent neurons in the head. Above the animal, a low-magnification light path captures images for behavior quantification (Fig. S6A). A live-tracking system keeps the animal centered in view as it freely moves. An automated data processing pipeline was used to extract GCaMP traces and behavioral variables from these videos[54]. We previously recorded animals expressing pan-neuronal NLS-GFP and NLS-mNeptune2.5 to estimate motion artifacts in data recorded on this imaging platform and found that they are negligible[54]. Nevertheless, we use GFP recordings to control for any small motion artifacts (see Methods).

As expected, animals abruptly slowed down upon food encounter (Fig. 6A–C). In addition, their oscillatory head movements slowed and their feeding rates increased (Fig. 6B). NSM was inactive while animals were off food, but activated upon food encounter and showed phasic bouts of activity while animals moved and ate (Fig. 6B, bottom). We examined whether NSM's ongoing activity was correlated with changes in speed, head movement, and feeding. To do so, we examined the correlation of NSM GCaMP to these behavioral variables when animals were on food. We favored this approach over an analysis that considers the off and on-food time epochs all at once, which would inevitably lead to

the conclusion that food-activated NSM is associated with all food-induced behaviors even if they are not convincingly time-locked to NSM. During this on-food time epoch, NSM activity showed negative correlations with speed and the rate of head bending and a positive correlation with feeding (Fig. 6H), matching the effects of optogenetic NSM stimulation (Fig. 1A).

We next examined brain-wide activity (example dataset in Fig. 6D). First, we determined the main modes of neural dynamics using principal component analysis (PCA), again analyzing the on-food epoch to focus on neural dynamics during serotonin release (Fig. 6E). In every dataset, one of the top three PCs was strongly correlated with NSM activity (Fig. 6E) and in most animals one of the other top PCs was correlated with the derivative of NSM activity (Fig. 6E). This suggests that NSM and its derivative are associated with a large portion of the variance in brain activity while animals feed.

To characterize these widespread changes more precisely, we examined how each neuron in each recording was related to NSM activity (example in Fig. 6F). The relationship between NSM and any other neuron could be instantaneous or time-lagged. Therefore, we convolved NSM's activity with a set of kernels that could result in NSM's original activity or temporally integrated versions of NSM activity (±10sec or less). For each neuron, we asked which of these convolved NSM traces was most strongly correlated with it and used shuffle controls to test for significance (see Methods). We also performed a parallel analysis that convolved NSM with kernels that took its derivative (NSM activity was not correlated with its own derivative, Fig. S6B–C). Across animals, 33% and 21% of the recorded neurons were significantly associated with NSM or its derivative, respectively (45% of neurons altogether). Negative correlations were more prevalent than positive ones (Fig. 6G). These results show that many neurons display activity patterns associated with NSM activity in heterogeneous ways: excitatory, inhibitory, time-lagged, or by tracking its derivative.

We asked which behavioral networks the NSM-associated neurons participate in by examining how their activity encoded behavior prior to NSM activation (Fig. 6F, bottom). This revealed that neurons that encoded forward velocity or head curvature prior to food encounter were significantly more likely to display activity that was inversely correlated with NSM after food encounter (Fig. 6I), suggesting that increased NSM activity was associated with inhibition of the locomotion and head movement networks.

Mapping NSM-associated brain dynamics onto the connectome

Finally, we mapped out which neurons in the connectome showed functional associations with NSM. To do so, we performed additional brain-wide recordings using a strain expressing pan-neuronal GCaMP7f and the NeuroPAL transgene (using *otIs670*, a low-brightness NeuroPAL integrant). After the freely-moving recordings, we immobilized animals and captured multi-spectral fluorescence. We then used NeuroPAL to determine neural identity and registered those images back to the freely-moving data.

The results from the NeuroPAL recordings were consistent with our other recordings. NSM activity was correlated with reduced speed and head movements and a similar fraction of neurons was associated with NSM (29% vs 33% above). We examined which neuron

classes showed reliable associations with NSM activity (Fig. 7A; Fig. S7A). Some sensory neurons showed positive correlations with NSM (AWB, BAG) while others showed negative correlations (AWC, OLQ). This suggests that changes in NSM activity are associated with bi-directional activity changes across different sensory channels. Pharyngeal neurons were significantly more likely to be positively correlated with NSM (Fig. 7B), consistent with the positive relationship between NSM and feeding behavior. We mapped our results onto the encoding properties of the neurons and found that locomotion- and head bending-encoding neurons were more likely to be negatively correlated with NSM and feeding-encoding neurons were more likely to be positively correlated (Fig. 7C). Thus, NSM-associated brain dynamics map onto functionally defined groups of neurons in the connectome in different ways.

We also examined whether the serotonin receptor expression profiles of neurons could predict their functional correlations with NSM. Neuron classes that were significantly associated with NSM were more likely to express at least one serotonin receptor (Fig. 7D; Fig. 7E, left). However, not all neurons followed this rule: some neurons with no receptors were correlated to NSM and some neurons with receptors showed no significant correlation (Fig. 7A). We also examined more detailed relationships: neurons expressing only excitatory serotonin receptors were more likely to be positively correlated with NSM, whereas neurons with inhibitory and excitatory receptors were more likely to be negatively correlated with NSM (Fig. 7E). However, despite these statistical trends, functional correlations with NSM still cannot be fully predicted by each neuron's serotonin receptor expression profile.

We also asked whether information about the presynaptic inputs onto a neuron class could provide additional information about whether its activity was associated with NSM. Neurons were significantly more likely to be associated with NSM if they received a higher fraction of synaptic inputs from neurons that expressed at least one serotonin receptor (Fig. 7F–G). This suggests that NSM-associated dynamics can be influenced by serotonin receptors expressed by a neuron's presynaptic inputs. Thus, synaptic transmission across the network further influences serotonin-associated brain dynamics.

DISCUSSION

Serotonin signaling influences behavior and cognition, but how serotonin acts through diverse receptor types to alter brain activity and behavior remains poorly understood. We examined this using a paradigm where we activated NSM, a feeding-responsive neuron whose extra-synaptic release of serotonin drives behavioral changes associated with foraging. A comprehensive analysis revealed how serotonin receptors mediate the effects of serotonin on behavior: one group of "driver" receptors induced slow locomotion and another group of "modulator" receptors further modified these behavioral changes. The MOD-1 and SER-4 driver receptors supported different dynamical changes in behavior and cell-specific genetic perturbations showed that the sites of expression of the distinct receptors played a key role in conferring their functional properties. Brain-wide calcium imaging in freely-moving animals revealed how serotonin release is associated with changes in activity across the defined cell types of the animal's brain. Sites of serotonin receptor expression can partially predict which neurons change activity during serotonin release, but

the pervasive brain-wide activity changes that accompany serotonin release extend beyond these cells to others in the network. Overall, these results provide a global view of how serotonin acts on a diverse set of receptors distributed across a connectome to modulate brain-wide activity and behavior.

NSM serotonin release alters locomotion in a manner that depends on all six serotonin receptors. By examining behavioral responses to serotonin release in a panel of mutants lacking every possible combination of serotonin receptors, we determined the logic of how the receptors interact to control behavior. Three serotonin receptors (SER-4, MOD-1, and LGC-50) drive the serotonin-induced locomotion change and three others (SER-1, SER-5, and SER-7) further modulate these effects. We identified specific patterns of redundancy and antagonism between combinations of these receptors, captured by a computational model. Understanding how a given serotonin receptor contributes to a behavioral output and how it interacts with the others will be critical to eventually target serotonin receptors in a rational way for therapeutics. In mammals, different serotonin receptor types have been suggested to influence different aspects of behavior and cognition[2,6,7], and complex interactions likely shape these functional roles.

The serotonin receptors that directly impact locomotion mediate responses to different patterns of serotonin release. Whereas MOD-1 activation induced sustained slowing during persistent NSM activation, SER-4 activation induced transient slowing in response to abrupt NSM activation. MOD-1 is an ionotropic receptor and SER-4 is a metabotropic receptor[47,48]. Although metabotropic receptors are classically thought to underlie sustained changes in cellular function, in this case the ionotropic receptor supports the sustained behavioral changes. We found that these distinct functions are due to the sites of expression of the receptors. However, the functional difference between the sets of neurons expressing these two receptors is currently unclear. It may involve their levels of recurrent connectivity or their underlying biophysics[55,56]. The finding that there are separable mechanisms that drive behavioral responses to abrupt changes in NSM activity and tonic NSM activity could have ethological significance. Sudden increases in NSM activity occur when animals suddenly encounter a better food source and continued tonic activity may allow animals to tune their locomotion to smaller environmental changes[36,37] (Fig. 1). Having both modes of responding may allow animals to maintain sensitivity to different environmental features.

We observed widespread dynamics across ~45% of the brain associated with ongoing changes in NSM activity. Our experiments did not distinguish which of these changes reflect the causal influence of NSM on downstream neurons, though NSM's extra-synaptic release of serotonin could account for many of these changes. In addition, recent studies revealed widespread *C. elegans* brain dynamics related to locomotion, so many of these changes could also be due to connectivity intrinsic to the locomotion network[54,57,58]. Activity in neurons in the networks that control locomotion and head curvature were inversely correlated with NSM activity, while activity in the feeding network was positively correlated. In mammals, there is also evidence of distinct serotonergic subsystems defined by anatomy and receptor expression that influence different aspects of behavior[8,10,29]. We found that patterns of serotonin receptor expression in a neuron and its presynaptic partners partially predicted which neurons were correlated with NSM. This suggests that

serotonin receptor expression patterns and synaptic interactions work together to shape serotonin-associated brain dynamics.

Even finer levels of resolution may be necessary to fully understand serotonergic modulation in *C. elegans*. For example, we observed a surprising level of co-expression of excitatory and inhibitory serotonin receptors in individual *C. elegans* neurons, which is also observed in mammals[59]. Such co-expression might enable fine tuning of serotonin responses in neurons. Alternatively, these receptors may localize to different cellular compartments[25]. This could allow separate synapses along a single neuron to be modulated differently by serotonin. The precise sites of action of each receptor, and the way that this modulation interacts with ongoing fast transmission, likely shape each receptor's role in modulating brain-wide activity and behavior.

LIMITATIONS OF THE STUDY

We highlight four potential limitations of our work. First, we examined the roles of the six *C. elegans* serotonin receptors that have been identified to date. Although the sextuple mutant lacking these receptors had no behavioral response to NSM serotonin release, this does not fully rule out the presence of additional receptors. Second, our whole-brain calcium imaging experiments revealed functional correlations between NSM and other neurons, but we did not directly test the causal influence of neurons on one another. Third, serotonin is only one of many neuromodulatory systems that influence *C. elegans* locomotion. However, the approaches we developed here can now be applied to other neuromodulatory systems to examine their functional organizations as well. Finally, the *C. elegans* connectome differs from that of other organisms in terms of size, connectivity, and emergent activity. Therefore, it may be challenging to immediately translate some findings to other organisms. However, the organizational principles learned here should still point to avenues of investigation.

STAR METHODS

RESOURCE AVAILABILITY

Lead Contact—Further information and requests for resources and reagents should be directed to and will be fulfilled by the lead contact, Steven Flavell (flavell@mit.edu).

Materials Availability—All plasmids, strains, and other reagents generated in this study are freely available upon request. Several key strains are also deposited in the Caenorhabditis Genetics Center (CGC).

Data and Code Availability

- **Data:** Data related to Figures 1–5 are freely available upon request. Behavioral and neural data related to Figure 6 and 7 have been deposited at Zenodo and Github and are publicly available as of the date of publication. DOIs are listed in the key resources table.
- **Code:** All original code has been deposited at Github and Zenodo and is publicly available as of the date of publication. DOIs are listed in the key resources table.

- Any additional information required to reanalyze the data reported in this work paper is available from the Lead Contact upon request.

EXPERIMENTAL MODEL AND SUBJECT DETAILS

C. elegans—*C. elegans* Bristol strain N2 was used as Wild-type. All wild-type, mutant and transgenic strains used in this study are listed in the Key Resources Table. Animals were maintained on NGM agar plates supplemented with *E. coli* OP50 bacteria strain. They were kept at room temperature (~22°C) and one day-old adult hermaphrodite animals were used for all experiments. For genetic crosses, genotypes were confirmed by PCR, sequencing, or Transnetyx genotyping. Transgenic animals were generated either by injecting DNA clones with fluorescent co-injection marker into the gonads of young adult hermaphrodites or CRISPR/Cas9.

METHOD DETAILS

Plasmids—A *tph-1*(short promoter fragment)::Chrimson plasmid that was previously described[37] was used to drive NSM::Chrimson expression. For transgenic expression of *ser-4* and *mod-1*, the *Y22D7AR.13.1* and *K06C4.6a.1* transcripts were amplified and subcloned into pSM-t2a-GFP. For Cre expression, the following promoters were subcloned into pSM-nCre (which has been previously described[35]): *rimb-1*, *unc-25, cat-1, nlp-70, ser-2b, tbh-1, ttx-3, flp-14, opt-3, ver-3, odr-2(2b)*.

New alleles of serotonin receptor genes—We engineered a new predicted null allele of *lgc-50* (*flv8*) using CRISPR/Cas9 gene editing. The mutation changes the sequence TCGAAGTGTTTC***GGC***AAGGATAACACTTG to TCGAAGTGTTTC***ACAGTTTCAGAGAAGTGTTGAG<u>TG</u>***AAGGATAACACTTG (a 3bp deletion and 24bp insertion; bold italics), which introduces an in-frame stop codon (underlined). This mutation is in exon 7, which encodes three of the transmembrane domains of the LGC-50 receptor, suggesting that this allele is likely to be a functional null.

We also engineered a new predicted null allele of *ser-4* (*flv7*) using CRISPR/Cas9 gene editing, because the site of integration for the NSM::Chrimson transgene (*flvIs2*) was closely linked to *ser-4*, such that we were unable to cross existing alleles of *ser-4* with *flvIs2*. The engineered mutation changes the sequence CCTGGAACCTCGG***CG***TCGTGGTCTGTGACTT to CCTGGAACCTCGG***TCTG<u>TGA</u>CT***TCGTGGTCTGTGA (a 2bp deletion and 9bp insertion; bold italics), which introduces an in-frame stop codon (underlined). This mutation is in exon 3 of the gene, which encodes two full transmembrane domains and part of a third, suggesting that this allele is likely to be a functional null.

Single-neuron calcium imaging of NSM—Single-neuron calcium imaging of NSM was performed as previously described[37]. One day old adult animals expressing GCaMP6m only in the NSM neuron were imaged under a widefield epifluorescence microscope using 10ms exposures at 10 fps. A 4x/0.2NA objective and Andor Zyla 4.2 Plus sCMOS camera were used for imaging. Animals were imaged on flat nematode growth media (NGM) agar pads seeded with *E. coli* OP50 bacteria as described in the main text. Agar imaging

pads were prepared immediately before imaging. Neurons were segmented and tracked using custom ImageJ scripts. For experiments with combined NSM::Chrimson stimulation, animals were grown on 5uM all-trans-retinal the night before, imaged at reduced blue light intensity while immobilized with 5mM tetramisole, and red light was delivered via a 617nm red LED light (Mightex).

NSM-induced locomotion behavioral assays—Locomotion recordings via multi-worm tracker during optogenetic stimulation were conducted using previously described methods[37,60]. L4 animals were picked to a 6 cm plate seeded with 200uL OP50 plus 50um ATR 16–24 hours prior to recording. The day of experiments, young adult animals were washed with 750 uL of M9 buffer twice and then placed on 10 cm plates. These 10 cm NGM plates had a thin filter paper ring dipped in 0.02M copper chloride solution. As heavy metals act as an aversive cue to the animals, this served to prevent animals roaming out of the camera's field of view. For 'fasted' condition experiments, animals were washed twice, then placed onto a 6 cm NGM plate with no bacterial lawn present. After 3 hours on this no-food plate, animals were washed twice and recorded immediately on the 10 cm NGM plate with no food.

Streampix software was used to record animals at 3 fps. 625nm light illumination from a Mightex LED was applied at defined times in the video. JAI SP-20000M-USB3 CMOS cameras (41mm, 5120×3840, Mono) with Nikon Micro-NIKKOR 55mm f/2.8 lenses were used. Backlighting was provided by a white panel LED (Metaphase Technologies Inc. White Metastandard 10" X 25," 24VDC). The recordings were analyzed via custom MATLAB scripts.

NSM-induced multi-behavioral assays—To record multiple *C. elegans* motor programs, we used a previously described custom microscopy system for single-worm tracking[61]. L4 animals were picked onto a 6 cm Nematode Growth Medium (NGM) plate seeded with 200 uL OP50 plus 50 um ATR. Animals fed on this plate in the dark overnight (12–24 hours). The next day, single one-day old adult animals were picked to a 10 cm NGM plate, which had a cut ring of thin film paper, which was soaked in 0.02M Copper Chloride solution. Animals were then placed on a custom tracking microscope that recorded brightfield images of the animal at 20 fps (detailed in Cermak et al[61]). A 532nm laser provided illumination at defined times in the video. Using custom R Studio scripts, velocity, pumping, head angle, defecation, and egg-laying were calculated for each animal. Custom MATLAB scripts were then used to compile and plot data.

To calculate head oscillations in Fig. 1, head angle data from each animal was analyzed in the spectral domain using the MATLAB Signal Processing Toolbox. To calculate head angle, the animal was divided into 500 equally spaced segments from nose to tail, and head angle was defined as bending around a pivot point at the 39th segment. For this analysis, cubic spline interpolation was used to generate points for small stretches of frames in which angle data was not recorded by the tracker (mean gap length was < 0.5sec; max gap length was 19.35sec). This was done in order to generate longer stretches of continuous data, which allowed us to achieve better frequency-domain resolution. For each recorded worm, the power spectral density estimate of the worm's head angle was calculated for each

individual laser-off time stretch using the multitaper method. These were then averaged across animals in order to obtain the average power spectral density during baseline behavior. During baseline behavior, we found a peak in power spectral density in the 0.3–0.7 Hz range, corresponding to the frequency of typical oscillatory off-food movement under standard recording conditions. We defined this frequency band as the “roaming band”. We then quantified the average signal power across these frequencies during laser-off and laser-on time stretches to quantify the animals’ head oscillations that accompany high speed movement.

Food encounter behavioral assays—The food patch encounter behavioral assay was adapted from previous work[37]. Wild-type and mutant animals were picked as L4s to 6mm plates with 200 ul OP50 lawn 16–24 hours prior to experiments. NGM was prepared in 86×128 mm plates (Thermo) and these plates were seeded with OP50 to create a bacterial lawn covering approximately 2/3 of the plate 16 hours before the recordings.

On the day of experiment, worms were gently washed twice with 750 ul M9 buffer to remove any bacterial residues. For the fed conditions, worms were then transferred to the assay plates for recording. For fasted conditions, worms were transferred to a 6mm plate without any OP50 and kept for 3 hours prior to recording.

Streampix software and the hardware described above were used to record animals at 3 fps for 1 hour. Videos were analyzed and data was plotted via custom MATLAB scripts.

Determining the identities of labeled neurons in the serotonin receptor expression reporter lines—The six T2A-mNeonGreen reporter strains were constructed by inserting a T2A-mNeonGreen coding sequence immediately before the stop codons of *mod-1, ser-1, ser-4, ser-5, ser-7* and *lgc-50* via CRISPR/Cas9 gene editing.

To determine the identities of neurons with serotonin receptor expression, each reporter line was crossed into the NeuroPAL strain. For imaging, one-day old adult animals were picked without any OP50 and immobilized on a flat NGM imaging pad with 100um sodium azide (Sigma Aldrich). Imaging was performed on a Zeiss LSM900 confocal microscope. Imaging parameters and neural identification strategies were conducted as described by Yemini et.al (2021).

Permutation tests related to receptor expression patterns—To calculate enrichment of serotonin receptors in the Rich Club[53], each stratum[52], and each neuron type, we conducted permutation tests. For a given group of interest G, (e.g. a specific stratum) of size N, we randomly selected N neurons from the pool of all relevant neurons. For the strata, this pool is the neuropil, for the Rich Club and neuron type it is the non-pharyngeal system. We noted the number of each of the six serotonin receptors in this random sample, $S_{i,r}$, where i is taken from the set {ser-1, ser-4, ser-5, ser-7, mod-1, lgc-50}. We compared the random observation to $S_{i,G}$, the number of each serotonin receptor in G. We repeated this random sampling 1000 times. The fraction of random samples for which $S_{i,r} > S_G$ provides an estimate of the likelihood of observing a value as high (or low) as $S_{i,G}$.

We calculated the likelihood of observing multiple serotonin receptors in the same single cells via a similar permutation test. For a given neuron containing two different serotonin receptors *i* and *j*, we noted the total number of each receptor in the whole network (non-pharyngeal system). We then randomly shuffled the locations of these receptors, such that the same number of receptors were placed across different neurons. We repeated this randomization 1000 times, and counted the number of instances where the serotonin receptors *i* and *j* co-occurred in the same neuron more often than in the real network.

Statistical comparison of well-fed and fasted animals—For Fig. 3C, we only considered there to be a difference between fed and fasted conditions if three criteria were met: (1) the loss of the receptor led to a different effect on behavior in well-fed and fasted animals (enhanced vs attenuated vs no-effect on NSM-stimulated locomotion); (2) the magnitude of the behavioral change due to loss of the receptor was significantly different between the fed and fasted conditions (since criterion (1) could be susceptible to p-values changing from 0.04 to 0.06, etc); and (3) these differences could be observed under conditions where neither parental group (i.e. the strain with the given serotonin receptor still intact) had saturating levels of slowing, since this would complicate interpretation of lack of an effect upon deletion of a receptor. Using these criteria, we observed many significant differences between fed and fasted animals, as is shown in the figure panel.

Linear model for how serotonin receptors interact to drive slow locomotion—We built a linear model to predict the level of NSM-induced slowing across the full panel of serotonin receptor mutants (64 total genotypes). The model with no interaction terms predicted the minimum speed of animals during NSM stimulation using an intercept and six predictor terms, one for each serotonin receptor gene indicating whether it was present (value=1) or absent (value=0) in a given genotype. This model and other versions of it described below were trained using L1-penalized (lasso) maximum likelihood fits, selecting the lambda (regularization) parameter that optimized the cross-validated performance for the particular model. For the linear model with interaction terms, these terms had the form of describing the joint presence of two or more serotonin receptors in a given genotype (for example, an interaction term could describe whether both *ser-4* and *mod-1* were present (value=1) versus if either or both receptors were absent (value=0)). We constructed a model with interaction terms in the following manner. The model initially contained no interaction terms (just the six predictor terms described above). We then asked whether interaction terms describing the joint presence of two receptors (all 2-mer combinations were tested) could be justified based on the data. To do so, we obtained model parameters for a model trained on 3 genotypes: the sextuple mutant and the two quintuple mutants with each of the two receptors (for the 2-mer in question) present. We then used these parameters to predict the level of slowing in the quadruple mutant with both receptors present and compared this to the data from actual animals. If these two values were significantly different (assessed with empirical p-value that the difference was non-zero), then the presence of an interaction term was justified and it was added to the model. If they were not significantly different, no interaction term was added to the model. After all 2-mers were evaluated, they were added to the model and included in a similar analysis to test whether addition of 3-mer interaction terms could be justified (i.e., this evaluation was based on a model that already included the

necessary 2-mer interaction terms, and asked whether beyond those any 3-mer interaction terms also needed to be added). This was iterated again for 4-mers. This iterative approach was chosen since it would favor simpler, more parsimonious interaction terms. Once this model was complete, we attempted to discard interaction terms that were not fully necessary in the full model. Specifically, terms that when trained on the full set of genotypes had coefficients that were not significantly different from zero (assessed with empirical p-value) were discarded. This was also to favor the simplest, most parsimonious model.

Modeling of dynamical behavioral responses to optogenetic NSM stimulation for *mod-1*-only and *ser-4*-only mutant animals—We constructed a model to predict the dynamics of animals' behavioral responses to optogenetic NSM stimulation. The aim of the model was to determine a set of parameters that fit *mod-1*-only mutants and *ser-4*-only mutants so that they could be compared, while accounting for potential floor/ceiling effects and more. Model parameters were trained on *mod-1*-only or *ser-4*-only behavioral data where NSM was stimulated with different light waveforms (8 different stimulation patterns), and then evaluated on behavioral data to 2 different stimulation patterns not included in the training data. Different splits of training/testing data gave similar results, and results for one split are shown in Fig. S4A. The model was:

$$\frac{ds}{dt}(t) = (\lambda_1 + \lambda_2 NSM(t)) \cdot (s_{target}(t) - s(t))$$
$$s_{target}(t) = \text{clamp}((K * NSM)(t), s_{min}, s_{max})$$
$$K(x) = \begin{cases} 0 & x > 0 \\ \tau e^{\tau x} - 1 & -1 < x \leq 0 \\ \tau e^{\tau x} & x \leq -1 \end{cases}$$
$$NSM(t) = \alpha \cdot \sigma(Stim(t), c, a)$$

$NSM(t)$ is the optogenetic stimulation pattern and $s(t)$ is the slowing of locomotion in response to the stimulus. s_{min} and s_{max} (set to the same values for all models) were set to match min and max speeds in real datasets, to allow the model to account for floor and ceiling effects. λ_1 and λ_2 were fit to account for the onset and offset of the locomotion change at NSM stimulation onset and offset. The sigmoid parameters (α, c, a) were fit to allow for scaling of the behavioral response to the NSM stimulation level. The τ parameter of the kernel was fit during training and its value determined whether the behavioral response to NSM stimulation weighed the current, absolute level of NSM stimulation versus the derivative of NSM stimulation. Lower values of τ favor weighing of the current, absolute level of NSM stimulation; higher values favor weighing of the derivative. To make the value of τ more intuitive, in Fig. S4A we display the shapes of the kernels that were fit for *mod-1*-only and *ser-4*-only animals, using the fit τ values. We also examined fits of control models where the kernel was constrained so that it could convolve recent NSM activity, but could not compute a difference (i.e. derivative). This led to extremely poor model performance on *ser-4*-only data and slightly worse performance on *mod-1*-only data.

Whole-brain calcium imaging recordings

Transgenic animals.: We recorded data from two transgenic strains that have been previously described. SWF415, which expresses: *flvIs17*: *rimb-1::NLS-GCaMP7f*, along

with *NLS-TagRFP-T* expressed under the followed promoters: *gcy-28.d, ceh-36, inx-1, mod-1, tph-1(short), gcy-5, gcy-7*; and *flvIs18*: *rimb-1::NLS-mNeptune2.5*. And SWF702, which expresses: *flvIs17*: described above; and *otIs670*: low-brightness NeuroPAL[50].

Microscope.: The microscope used for brain-wide calcium imaging has been previously described[41,54]. Briefly, the microscope simultaneously images the animal via two light paths, one above and one below the animal. The light path used for all fluorescence imaging is an Andor spinning disk confocal system, containing a 5000 rpm Yokogawa CSU-X1 spinning disk unit and Borealis upgrade, built on a Nikon ECLIPSE Ti microscope. Laser lines were: 150 mW 488 nm laser, 50 mW 560 nm laser, 100 mW 405 nm laser, or 140 mW 637 nm laser. A 40x water immersion objective (CFI APO LWD 40X WI 1.15 NA LAMBDA S, Nikon) with an objective piezo (P-726 PIFOC, Physik Instrumente (PI)) was used to image the volume of the worm's head. A quad dichroic mirror directed light emitted from the specimen to two separate sCMOS cameras (Andor Zyla 4.2 PLUS sCMOS), which had in-line emission filters (525/50 for GCaMP/GFP, and 610 longpass for mNeptune2.5; NeuroPAL filters described below). Data was collected at 3 × 3 binning in a 322 × 210 region of interest in the center of the field of view, with 80 z planes collected at a spacing of 0.54 um, resulting in a volume rate of 1.7 Hz.

The light path for behavior imaging was in a reflected brightfield (NIR) configuration. Light from a 850-nm LED (M850L3, Thorlabs) was collimated and passed through a 850/10 bandpass filter (FBH850–10, Thorlabs). Illumination light was reflected towards the sample by a half mirror and was focused on the sample through a 10x objective (CFI Plan Fluor 10x, Nikon). Image from the sample passed through the half mirror and was filtered by another 850-nm bandpass filter of the same model. The image is captured by a CMOS camera (BFS-U3–28S5M-C, FLIR).

The microscope utilized a closed-loop tracking system to keep the animal in view. For closed-loop tracking, NIR brightfield images were analyzed at a rate of 40 Hz to determine the location of the worm's head, identified via a custom-trained network with transfer learning using DeepLabCut[62]. This network identified the location of three key points in the worm's head (nose, metacorpus of pharynx, and grinder of pharynx). The tracking target that was kept centered in the field of view was a point halfway between the metacorpus and grinder (central location of neuronal cell bodies). Additional details are available in the original article to report this microscope.

Recording procedure.: Animals were raised on *E. coli* OP50 and imaged as one day-old adults. Each animal was mounted on a thin, flat agar pad (2.5 cm × 1.8 cm × 0.8 mm) with NGM containing 2.2% agar. *E. coli* OP50 that had been seeded on agar plates 3 days beforehand was spread on the agar pad with a sterile inoculating loop (Thermo Scientific), after which 4 uL of M9 buffer was added to the center of the agar pad. The animal was then transferred to the drop of M9 buffer. At each corner of the agar pad, 1 uL of 80 um microbeads suspended in M9 buffer were added as vertical spacers, on top of which a #1.5 glass coverslip was added.

Each SWF415 animal was starved for 3 hours before the mounting procedure. *E. coli* OP50 was spread along three sides of the agar pad such that the animal is ~0.6 cm away from each lawn boundary. The glass coverslip was lowered gently from the foodless side in order to avoid contaminating the central foodless zone with *E. coli* OP50. Imaging was performed 3 minutes after the mounting procedure to allow for habituation to the sensory environment.

Each SWF702 animal was starved for 1.5–2 hours before the mounting procedure. *E. coli* OP50 was spread evenly to form a circular lawn of 0.5 cm diameter, and the animal was mounted at the center of the food lawn. Imaging was performed immediately after the mounting procedure to capture the initial phase of food-induced neural activity.

Data processing.: Whole-brain GCaMP/mNeptune2.5 data were processed into normalized calcium traces using the Automated Neuron Tracking System for Unconstrained Nematodes (ANTSUN) data processing pipeline that we have previously described[54]. Briefly, this software package uses the mNeptune2.5 signal to identify the neurons in all frames and to register volumes from different time points to one another. The end result is a Fluorescence (F) measurement for each neuron, which is the ratio of GCaMP7F signal divided by mNeptune2.5 signal for that neuron. Behavioral data were extracted from the NIR videos using previously described methods.

Procedure for NeuroPAL imaging.: NeuroPAL recording procedures were carried out as previously described[54]. Briefly, animals were imaged immobilized by cooling immediately after the freely-moving recording ended. A closed-loop temperature controller (TEC200C, Thorlabs) with a micro-thermistor (SC30F103A, Amphenol) embedded in the agar was used to keep the agar temperature at the 1 °C set point. This allowed us to capture a series of multi-spectral images at longer exposure times (15–20 ms per z-slice) for NeuroPAL-based neural identification:

(1–3) Spectrally isolated images of mTagBFP2, CyOFP1, and mNeptune2.5. CyOFP1 data was collected with 488nm laser excitation under a 585/40m bandpass filter. mNeptune2.5 was collected with 637nm laser excitation and a 655LP-TRF filter. mTagBFP2 was isolated with 405nm laser excitation and a 447/60m bandpass filter.

(4) An image with TagRFP-T, CyOFP1, and mNeptune2.5 (all of the “red” markers) in one channel, and GCaMP7f in the other channel. This image was used for neuronal segmentation and registration to both the freely moving recording and individually isolated marker images. For this image, we used 488nm and 561nm laser excitation. TagRFP-T, mNeptune2.5, and CyOFP1 were imaged with a 570LP filter and GCaMP6f was isolated using a 525/50m bandpass filter.

All images were recorded for 60 timepoints. We increased the signal to noise ratio for each of the images by first registering all timepoints within a recording to one another and then averaging the transformed images. Finally, we created the composite, 3-dimensional RGB image by setting the mTagBFP2 image to blue, CyOFP1 image to green, and mNeptune2.5 image to red as done by Yemini et al[50] and manually adjusting the intensity of each channel to optimally match their manual.

The neuron segmentation U-Net used in the ANTSUN pipeline was run on the “all red” image and we then determined the identities of U-net identified neurons using the NeuroPAL instructions. In some cases, neuronal identities could not be determined with certainty due a number of factors including: unexpectedly dim expression of one or more fluorophores, unexpected expression of a fluorophore in cells not stated to express a given marker, and extra cells in a region expressing similar intensities when no other cells are expected. In the rare occasion that multiple cells were labeled as potential candidates for a given neuron, the most likely candidate (based on position, coloring, and marker intensity) was used for analysis.

Finally, the neural identity labels from the RGB image were mapped back to the GCaMP traces from the freely-moving animal by first registering each fluorophore-isolated image to the image containing all of the red markers. The “all red” image was then registered back to the freely moving recording, permitting mapping of neuronal labels back to GCaMP traces.

Whole-brain calcium imaging data analysis

Principal Component Analysis (PCA).: To determine the main modes of neural dynamics in our recordings, we performed PCA on our neural datasets. To do so, we used the F/F_{20} GCaMP traces and performed PCA on all traces from a given recording using the post-food-encounter time epoch. Analyzing the full datasets (on-food and off-food epochs combined) gave rise to qualitatively similar results, but it was more obvious that the PCs arising from that analysis would be related to NSM, which is activated by feeding. By performing the analysis on only the on-food epoch, we were able to assess whether ongoing brain dynamics on food were related to NSM activity. To relate the resulting principal components to NSM, we performed the analysis described below for single neurons. However, instead of relating NSM to another’s neuron’s GCaMP signal, we correlated NSM activity to each principal component that explained >2% of the overall variance in neural activity.

Statistical procedure to determine how NSM activity is associated with behavior.: For each brain-wide recording, we examined whether NSM activity was associated with ongoing behavioral changes. Here, we focused on the relationship between NSM and behavior only in the on-food time epoch. This is because NSM is activated by feeding and analyzing all data (on-food and off-food time epochs combined) could potentially lead to the spurious conclusion that NSM is correlated with all feeding-induced behaviors, even when the time-locked association is weak. By focusing on the on-food epoch, we were able to ask whether ongoing changes in NSM activity were precisely associated with ongoing behavioral changes. We examined NSM’s relationship to five behavioral variables: velocity, speed, head curvature, head movement (absolute value of derivative of head curvature), and feeding (i.e. pharyngeal pumping rate). For each behavior, we performed the following analysis. First, we determined the Spearman correlation between NSM activity and the behavioral variable. To test whether the observed correlation coefficient exceeded values expected by random chance, we compared this value to a distribution of shuffle controls. This distribution was created by obtaining the correlation coefficients between shuffled, synthetic NSM traces and the behavioral variable being tested. The idea is that the shuffled, synthetic traces would preserve the temporal properties of NSM activity (autocorrelative

structure, etc), but would be completely de-synced from the behavior so that they estimate the level of correlation expected by chance. The shuffled, synthetic traces were obtained by building an encoding model that accurately predicts NSM GCaMP based on animal velocity (using the procedure in Atanas et al[54]). We then used random samples of velocity traces from animals recorded under similar conditions (we ensured the random velocity samples followed the same statistical distribution as that of the actual animals) to synthesize NSM traces and used these for the shuffle controls. Finally, we then determined the empirical p-value of the actual correlation coefficient based on its rank in the control distribution. We favored this approach over the more standard approach of temporally shifting NSM activity relative to behavior, because NSM has a very long autocorrelation, so to obtain independent shifted versions of NSM, its trace needs to be shifted by >100sec. Given the durations of our recordings, this makes it infeasible to obtain a sufficient number of independent, shifted NSM traces to perform statistical testing (at least 1000 required to achieve sufficient power). To ensure that the statistical test was valid, we performed control analyses where we examined whether actual NSM neurons from one animal were correlated to the behaviors of other animals, and found that for all permutations of this test they were not correlated.

Statistical procedure to determine how each neuron's activity is associated with NSM activity.: To test whether NSM activity in a given recording was associated with the activity of other simultaneously recorded neurons, we performed the following analysis. First, we only considered neurons for analysis if their signal variation, measured as standard deviation of their F/F_{20} signal, exceeded a value determined to be the boundary between real dynamics and measurement or motion noise. This value was determined based on an analysis of signal variation in the recordings where GFP was recorded in place of GCaMP. All GFP-expressing neurons fell below this value and only <15% of GCaMP neurons were excluded based on this criterion. These neurons were likely inactive under our recording conditions. Next, we wanted to allow for the possibility that NSM could have slightly lagged relationships to other neurons in the data. Thus, we first convolved the activity of NSM with a set of temporal kernels that could integrate NSM activity up to 10sec in the past or future. There were 20 such kernels, and therefore this resulted in 20 kernel-convolved NSM traces. Then, for a given neuron of interest, we determined which kernel-convolved NSM trace had the strongest correlation with the neuron. Then, to test whether this correlation coefficient was significant, we used the procedure described in the above paragraph (for NSM vs behavior analyses) where we obtained a distribution of shuffle controls. For these controls, each shuffled, synthetic NSM trace was put through the same procedure. The idea is that these traces have the temporal properties of NSM activity, but should be completely de-synced from the neuron being analyzed so that this estimates the level of correlation expected by chance. Importantly, the shuffled, synthetic NSM traces were all convolved with the same filters and the highest possible correlation coefficient was the one added to the control distribution. We then determined the empirical p-value of the actual correlation coefficient based on its rank in the control distribution. Multiple comparison correction was applied across all neurons in each dataset using Benjamini-Hochberg set to FDR<0.1. We also implemented a second requirement for neurons to be considered as significantly associated with NSM. Specifically, we aimed to exclude neurons where the variance explained by its correlation with NSM was not separable from levels of measurement or motion artifact

noise. To estimate this, we utilized a set of recordings where NLS-GFP was recorded instead of NLS-GCaMP. For each GFP-expressing neuron, we attempted to explain its activity with NSM GCaMP from another recording and then estimated the variance explained in the GFP signal by NSM. This was a typically small number that clearly reflects noise. We selected a threshold for this number that exceeded >95% of these control measurements. Then, for each actual neuron simultaneously recorded with NSM that passed the shuffle test, we asked whether the variance explained by its correlation with NSM exceeded this threshold value. If it did not, the neuron was not considered to be significantly associated with NSM.

In parallel, we performed an identical analysis using a series of differentiator kernels that compute the derivative of NSM over 10 sec or less. Four possible kernels were used for this purpose. Otherwise, the procedure was identical to the one described above. For both tests, we ran control analyses to ensure the validity of the tests, in which we asked whether NSM from one animal could be correlated to the neurons from another animal and found that <5% of neurons were significant for these analyses (vs 44.9% in actual analyses). All statistical analyses of the whole-brain imaging data were performed using Julia 1.8.0.

Determining the encoding properties of recorded neurons.: For many of our recordings, it was of interest to determine how each recorded neuron “encoded” behavior. “Encoded” here is defined as displayed GCaMP dynamics that were associated with the behavior. To perform this analysis, we used a previously-described statistical method[54]. A detailed description can be found in the cited study, but the conceptual framework is also described here. Briefly, we attempted to fit each recorded neuron with a probabilistic encoding model that attempts to use behavioral predictor terms (for velocity, movement direction, head curvature, and feeding) to describe the neuron’s activity. The form of the model allows neurons to encode behavior over varying timescales and potentially represent multiple behaviors. We fit the model using the probabilistic computing so that we can determine the full posterior distribution of model parameters that could explain the neural/behavioral data. This allows us to establish our confidence in a given model parameter, for example the parameter that explains how much the neuron’s activity reflects head curvature. Finally, we use these posterior distributions to test for significance. In this study, we asked whether each neuron significantly encoded: forward velocity, reverse velocity, dorsal head curvature, ventral head curvature, feeding (in a positive-correlated manner), and feeding (in a negative-correlated manner). To do so, we evaluated all of the points in the posterior distribution, asking whether that set of model parameters indicates tuning to the behavioral parameter of interest (for example, higher activity during forward versus reverse velocity). We then ask whether the null hypothesis of no significant tuning can be rejected (FDR<0.05), by examining the results from all points in the posterior.

Connectome analysis.: For analyses that relate synaptic wiring to brain activity, we utilized information from the *C. elegans* connectome. We used the electron microscopy annotations from White et al[31] and Witvliet et al[32] (3 adult hermaphrodites total). For each neuron class, the number of chemical and electrical synapses in each connectomic dataset was counted and summed across left/ right pairs to represent the total number of synapses made by the neuron (in each connectome). For all head neurons, the fraction of presynaptic inputs (a

metric used in Fig. 7) was the average value observed across the three connectomes. For all pharyngeal neurons, the fraction of presynaptic inputs was computed from a single animal in White et al[31] since that is the only connectome of the pharynx. Neuron classes with only connectome but not calcium recording information (e.g. ventral cord and tail neurons) were still considered when computing the fraction of synaptic inputs, but omitted from the analysis of relationships between a neuron class' NSM association and the properties of its presynaptic inputs.

QUANTIFICATION AND STATISTICAL ANALYSIS

All statistical analyses are described in the figure legends and, if indicated in the legends, additional details are in the Method Details section. Precise definitions of sample sizes, as well as definitions of center and dispersion and precision measures, are also provided in figure legends. Statistics were computed using MATLAB or GraphPad Prism. Non-parametric statistics were mostly used; when parametric tests were used, the D'Agostino-Pearson test was used to test data for normality. Multiple comparison corrections were made via Bonferroni correction or Benjamini-Hochberg, as described in the figure legends.

Supplementary Material

Refer to Web version on PubMed Central for supplementary material.

ACKNOWLEDGMENTS

We thank Matthew Lovett-Barron, Qiang Liu, Cori Bargmann, and members of the Flavell lab for comments on the manuscript. We thank the Caenorhabditis Genetics Center (P40 OD010440) and Oliver Hobert for sharing strains. E.T. acknowledges funding from NFRF (NFRFE-2021-00420) and NSERC (#RGPIN-2021-02949). M.A.G. was supported by NIH (GM135413-03S1). S.W.F. acknowledges funding from NIH (GM135413); NSF (Award #1845663); the McKnight Foundation; Alfred P. Sloan Foundation; The Picower Institute for Learning and Memory; and The JPB Foundation.

INCLUSION AND DIVERSITY

One or more of the authors of this paper self-identifies as an underrepresented ethnic minority in their field of research or within their geographical location. One or more of the authors of this paper self-identifies as a gender minority in their field of research. One or more of the authors of this paper self-identifies as a member of the LGBTQIA+ community. One or more of the authors of this paper received support from a program designed to increase minority representation in their field of research.

REFERENCES

1. Lin S-H, Lee L-T, and Yang YK (2014). Serotonin and mental disorders: a concise review on molecular neuroimaging evidence. Clin. Psychopharmacol. Neurosci. Off. Sci. J. Korean Coll. Neuropsychopharmacol. 12, 196–202. 10.9758/cpn.2014.12.3.196.
2. Yohn CN, Gergues MM, and Samuels BA (2017). The role of 5-HT receptors in depression. Mol. Brain 10, 28. 10.1186/s13041-017-0306-y. [PubMed: 28646910]
3. Madsen MK, Fisher PM, Burmester D, Dyssegaard A, Stenbæk DS, Kristiansen S, Johansen SS, Lehel S, Linnet K, Svarer C, et al. (2019). Psychedelic effects of psilocybin correlate with serotonin 2A receptor occupancy and plasma psilocin levels. Neuropsychopharmacol. Off. Publ. Am. Coll. Neuropsychopharmacol. 44, 1328–1334. 10.1038/s41386-019-0324-9.

4. Kraehenmann R, Pokorny D, Vollenweider L, Preller KH, Pokorny T, Seifritz E, and Vollenweider FX (2017). Dreamlike effects of LSD on waking imagery in humans depend on serotonin 2A receptor activation. Psychopharmacology (Berl.) 234, 2031–2046. 10.1007/s00213-017-4610-0. [PubMed: 28386699]
5. Hillhouse TM, and Porter JH (2015). A brief history of the development of antidepressant drugs: from monoamines to glutamate. Exp. Clin. Psychopharmacol. 23, 1–21. 10.1037/a0038550. [PubMed: 25643025]
6. Donaldson ZR, Nautiyal KM, Ahmari SE, and Hen R (2013). Genetic approaches for understanding the role of serotonin receptors in mood and behavior. Curr. Opin. Neurobiol. 23, 399–406. 10.1016/j.conb.2013.01.011. [PubMed: 23385115]
7. Barnes NM, and Sharp T (1999). A review of central 5-HT receptors and their function. Neuropharmacology 38, 1083–1152. 10.1016/s0028-3908(99)00010-6. [PubMed: 10462127]
8. Okaty BW, Commons KG, and Dymecki SM (2019). Embracing diversity in the 5-HT neuronal system. Nat. Rev. Neurosci. 20, 397–424. 10.1038/s41583-019-0151-3. [PubMed: 30948838]
9. Okaty BW, Sturrock N, Escobedo Lozoya Y, Chang Y, Senft RA, Lyon KA, Alekseyenko OV, and Dymecki SM (2020). A single-cell transcriptomic and anatomic atlas of mouse dorsal raphe Pet1 neurons. eLife 9, e55523. 10.7554/eLife.55523. [PubMed: 32568072]
10. Ren J, Friedmann D, Xiong J, Liu CD, Ferguson BR, Weerakkody T, DeLoach KE, Ran C, Pun A, Sun Y, et al. (2018). Anatomically Defined and Functionally Distinct Dorsal Raphe Serotonin Sub-systems. Cell 175, 472–487.e20. 10.1016/j.cell.2018.07.043. [PubMed: 30146164]
11. Ren J, Isakova A, Friedmann D, Zeng J, Grutzner SM, Pun A, Zhao GQ, Kolluru SS, Wang R, Lin R, et al. (2019). Single-cell transcriptomes and whole-brain projections of serotonin neurons in the mouse dorsal and median raphe nuclei. eLife 8, e49424. 10.7554/eLife.49424. [PubMed: 31647409]
12. Cohen JY, Amoroso MW, and Uchida N (2015). Serotonergic neurons signal reward and punishment on multiple timescales. eLife 4, e06346. 10.7554/eLife.06346. [PubMed: 25714923]
13. Grossman CD, Bari BA, and Cohen JY (2022). Serotonin neurons modulate learning rate through uncertainty. Curr. Biol. CB 32, 586–599.e7. 10.1016/j.cub.2021.12.006. [PubMed: 34936883]
14. Li Y, Zhong W, Wang D, Feng Q, Liu Z, Zhou J, Jia C, Hu F, Zeng J, Guo Q, et al. (2016). Serotonin neurons in the dorsal raphe nucleus encode reward signals. Nat. Commun. 7, 10503. 10.1038/ncomms10503. [PubMed: 26818705]
15. Marques JC, Li M, Schaak D, Robson DN, and Li JM (2020). Internal state dynamics shape brainwide activity and foraging behaviour. Nature 577, 239–243. 10.1038/s41586-019-1858-z. [PubMed: 31853063]
16. Paquelet GE, Carrion K, Lacefield CO, Zhou P, Hen R, and Miller BR (2022). Single-cell activity and network properties of dorsal raphe nucleus serotonin neurons during emotionally salient behaviors. Neuron 110, 2664–2679.e8. 10.1016/j.neuron.2022.05.015. [PubMed: 35700737]
17. Weissbourd B, Ren J, DeLoach KE, Guenthner CJ, Miyamichi K, and Luo L (2014). Presynaptic partners of dorsal raphe serotonergic and GABAergic neurons. Neuron 83, 645–662. 10.1016/j.neuron.2014.06.024. [PubMed: 25102560]
18. Cazettes F, Reato D, Morais JP, Renart A, and Mainen ZF (2021). Phasic Activation of Dorsal Raphe Serotonergic Neurons Increases Pupil Size. Curr. Biol. CB 31, 192–197.e4. 10.1016/j.cub.2020.09.090. [PubMed: 33186549]
19. Lottem E, Banerjee D, Vertechi P, Sarra D, Lohuis MO, and Mainen ZF (2018). Activation of serotonin neurons promotes active persistence in a probabilistic foraging task. Nat. Commun. 9, 1000. 10.1038/s41467-018-03438-y. [PubMed: 29520000]
20. Seo C, Guru A, Jin M, Ito B, Sleezer BJ, Ho Y-Y, Wang E, Boada C, Krupa NA, Kullakanda DS, et al. (2019). Intense threat switches dorsal raphe serotonin neurons to a paradoxical operational mode. Science 363, 538–542. 10.1126/science.aau8722. [PubMed: 30705194]
21. Schweighofer N, Bertin M, Shishida K, Okamoto Y, Tanaka SC, Yamawaki S, and Doya K (2008). Low-serotonin levels increase delayed reward discounting in humans. J. Neurosci. Off. J. Soc. Neurosci. 28, 4528–4532. 10.1523/JNEUROSCI.4982-07.2008.

22. Crockett MJ, Clark L, Tabibnia G, Lieberman MD, and Robbins TW (2008). Serotonin modulates behavioral reactions to unfairness. Science 320, 1739. 10.1126/science.1155577. [PubMed: 18535210]
23. Seymour B, Daw ND, Roiser JP, Dayan P, and Dolan R (2012). Serotonin selectively modulates reward value in human decision-making. J. Neurosci. Off. J. Soc. Neurosci. 32, 5833–5842. 10.1523/JNEUROSCI.0053-12.2012.
24. Bocchio M, McHugh SB, Bannerman DM, Sharp T, and Capogna M (2016). Serotonin, Amygdala and Fear: Assembling the Puzzle. Front. Neural Circuits 10, 24. 10.3389/fncir.2016.00024. [PubMed: 27092057]
25. Puig MV, and Gulledge AT (2011). Serotonin and prefrontal cortex function: neurons, networks, and circuits. Mol. Neurobiol. 44, 449–464. 10.1007/s12035-011-8214-0. [PubMed: 22076606]
26. Goodfellow NM, Benekareddy M, Vaidya VA, and Lambe EK (2009). Layer II/III of the prefrontal cortex: Inhibition by the serotonin 5-HT1A receptor in development and stress. J. Neurosci. Off. J. Soc. Neurosci. 29, 10094–10103. 10.1523/JNEUROSCI.1960-09.2009.
27. Béïque J-C, Imad M, Mladenovic L, Gingrich JA, and Andrade R (2007). Mechanism of the 5-hydroxytryptamine 2A receptor-mediated facilitation of synaptic activity in prefrontal cortex. Proc. Natl. Acad. Sci. U. S. A. 104, 9870–9875. 10.1073/pnas.0700436104. [PubMed: 17535909]
28. Puig MV, Watakabe A, Ushimaru M, Yamamori T, and Kawaguchi Y (2010). Serotonin modulates fast-spiking interneuron and synchronous activity in the rat prefrontal cortex through 5-HT1A and 5-HT2A receptors. J. Neurosci. Off. J. Soc. Neurosci. 30, 2211–2222. 10.1523/JNEUROSCI.3335-09.2010.
29. Salvan P, Fonseca M, Winkler AM, Beauchamp A, Lerch JP, and Johansen-Berg H (2023). Serotonin regulation of behavior via large-scale neuromodulation of serotonin receptor networks. Nat. Neurosci. 26, 53–63. 10.1038/s41593-022-01213-3. [PubMed: 36522497]
30. Cook SJ, Jarrell TA, Brittin CA, Wang Y, Bloniarz AE, Yakovlev MA, Nguyen KCQ, Tang LT-H, Bayer EA, Duerr JS, et al. (2019). Whole-animal connectomes of both Caenorhabditis elegans sexes. Nature 571, 63–71. 10.1038/s41586-019-1352-7. [PubMed: 31270481]
31. White JG, Southgate E, Thomson JN, and Brenner S (1986). The structure of the nervous system of the nematode Caenorhabditis elegans. Philos. Trans. R. Soc. Lond. B. Biol. Sci. 314, 1–340. [PubMed: 22462104]
32. Witvliet D, Mulcahy B, Mitchell JK, Meirovitch Y, Berger DR, Wu Y, Liu Y, Koh WX, Parvathala R, Holmyard D, et al. (2021). Connectomes across development reveal principles of brain maturation. Nature 596, 257–261. 10.1038/s41586-021-03778-8. [PubMed: 34349261]
33. Chase DL, and Koelle MR (2007). Biogenic amine neurotransmitters in C. elegans. WormBook Online Rev. C Elegans Biol, 1–15. 10.1895/wormbook.1.132.1.
34. Taylor SR, Santpere G, Weinreb A, Barrett A, Reilly MB, Xu C, Varol E, Oikonomou P, Glenwinkel L, McWhirter R, et al. (2021). Molecular topography of an entire nervous system. Cell 184, 4329–4347.e23. 10.1016/j.cell.2021.06.023. [PubMed: 34237253]
35. Flavell SW, Pokala N, Macosko EZ, Albrecht DR, Larsch J, and Bargmann CI (2013). Serotonin and the Neuropeptide PDF Initiate and Extend Opposing Behavioral States in C. elegans. Cell 154, 1023–1035. 10.1016/j.cell.2013.08.001. [PubMed: 23972393]
36. Iwanir S, Brown AS, Nagy S, Najjar D, Kazakov A, Lee KS, Zaslaver A, Levine E, and Biron D (2016). Serotonin promotes exploitation in complex environments by accelerating decision-making. BMC Biol. 14, 9. 10.1186/s12915-016-0232-y. [PubMed: 26847342]
37. Rhoades JL, Nelson JC, Nwabudike I, Yu SK, McLachlan IG, Madan GK, Abebe E, Powers JR, Colón-Ramos DA, and Flavell SW (2019). ASICs Mediate Food Responses in an Enteric Serotonergic Neuron that Controls Foraging Behaviors. Cell 176, 85–97.e14. 10.1016/j.cell.2018.11.023. [PubMed: 30580965]
38. Sawin ER, Ranganathan R, and Horvitz HR (2000). C. elegans locomotory rate is modulated by the environment through a dopaminergic pathway and by experience through a serotonergic pathway. Neuron 26, 619–631. 10.1016/s0896-6273(00)81199-x. [PubMed: 10896158]
39. Flavell SW, Raizen DM, and You Y-J (2020). Behavioral States. Genetics 216, 315–332. 10.1534/genetics.120.303539. [PubMed: 33023930]

40. Flavell SW, and Gordus A (2022). Dynamic functional connectivity in the static connectome of Caenorhabditis elegans. Curr. Opin. Neurobiol. 73, 102515. 10.1016/j.conb.2021.12.002. [PubMed: 35183877]
41. Ji N, Madan GK, Fabre GI, Dayan A, Baker CM, Kramer TS, Nwabudike I, and Flavell SW (2021). A neural circuit for flexible control of persistent behavioral states. eLife 10, e62889. 10.7554/eLife.62889. [PubMed: 34792019]
42. Nelson JC, and Colón-Ramos DA (2013). Serotonergic neurosecretory synapse targeting is controlled by netrin-releasing guidepost neurons in Caenorhabditis elegans. J. Neurosci. Off. J. Soc. Neurosci. 33, 1366–1376. 10.1523/JNEUROSCI.3471-12.2012.
43. Morud J, Hardege I, Liu H, Wu T, Choi M-K, Basu S, Zhang Y, and Schafer WR (2021). Deorphanization of novel biogenic amine-gated ion channels identifies a new serotonin receptor for learning. Curr. Biol. CB 31, 4282–4292.e6. 10.1016/j.cub.2021.07.036. [PubMed: 34388373]
44. Gürel G, Gustafson MA, Pepper JS, Horvitz HR, and Koelle MR (2012). Receptors and other signaling proteins required for serotonin control of locomotion in Caenorhabditis elegans. Genetics 192, 1359–1371. 10.1534/genetics.112.142125. [PubMed: 23023001]
45. Churgin MA, McCloskey RJ, Peters E, and Fang-Yen C (2017). Antagonistic Serotonergic and Octopaminergic Neural Circuits Mediate Food-Dependent Locomotory Behavior in Caenorhabditis elegans. J. Neurosci. Off. J. Soc. Neurosci. 37, 7811–7823. 10.1523/JNEUROSCI.2636-16.2017.
46. McLachlan IG, Kramer TS, Dua M, DiLoreto EM, Gomes MA, Dag U, Srinivasan J, and Flavell SW (2022). Diverse states and stimuli tune olfactory receptor expression levels to modulate food-seeking behavior. eLife 11, e79557. 10.7554/eLife.79557. [PubMed: 36044259]
47. Olde B, and McCombie WR (1997). Molecular cloning and functional expression of a serotonin receptor from Caenorhabditis elegans. J. Mol. Neurosci. MN 8, 53–62. 10.1007/BF02736863. [PubMed: 9061615]
48. Ranganathan R, Cannon SC, and Horvitz HR (2000). MOD-1 is a serotonin-gated chloride channel that modulates locomotory behaviour in C. elegans. Nature 408, 470–475. 10.1038/35044083. [PubMed: 11100728]
49. Hobson RJ, Hapiak VM, Xiao H, Buehrer KL, Komuniecki PR, and Komuniecki RW (2006). SER-7, a Caenorhabditis elegans 5-HT7-like receptor, is essential for the 5-HT stimulation of pharyngeal pumping and egg laying. Genetics 172, 159–169. 10.1534/genetics.105.044495. [PubMed: 16204223]
50. Yemini E, Lin A, Nejatbakhsh A, Varol E, Sun R, Mena GE, Samuel ADT, Paninski L, Venkatachalam V, and Hobert O (2021). NeuroPAL: A Multicolor Atlas for Whole-Brain Neuronal Identification in C. elegans. Cell 184, 272–288.e11. 10.1016/j.cell.2020.12.012. [PubMed: 33378642]
51. Brittin CA, Cook SJ, Hall DH, Emmons SW, and Cohen N (2021). A multi-scale brain map derived from whole-brain volumetric reconstructions. Nature 591, 105–110. 10.1038/s41586-021-03284-x. [PubMed: 33627874]
52. Moyle MW, Barnes KM, Kuchroo M, Gonopolskiy A, Duncan LH, Sengupta T, Shao L, Guo M, Santella A, Christensen R, et al. (2021). Structural and developmental principles of neuropil assembly in C. elegans. Nature 591, 99–104. 10.1038/s41586-020-03169-5. [PubMed: 33627875]
53. Towlson EK, Vértes PE, Ahnert SE, Schafer WR, and Bullmore ET (2013). The rich club of the C. elegans neuronal connectome. J. Neurosci. Off. J. Soc. Neurosci. 33, 6380–6387. 10.1523/JNEUROSCI.3784-12.2013.
54. Atanas AA, Kim J, Wang Z, Bueno E, Becker M, Kang D, Park J, Estrem C, Kramer TS, Baskoylu S, et al. (2022). Brain-wide representations of behavior spanning multiple timescales and states in C. elegans. Preprint at bioRxiv, 10.1101/2022.11.11.516186.
55. Jiang J, Su Y, Zhang R, Li H, Tao L, and Liu Q (2022). C. elegans enteric motor neurons fire synchronized action potentials underlying the defecation motor program. Nat. Commun. 13, 2783. 10.1038/s41467-022-30452-y. [PubMed: 35589790]
56. Liu Q, Kidd PB, Dobosiewicz M, and Bargmann CI (2018). C. elegans AWA Olfactory Neurons Fire Calcium-Mediated All-or-None Action Potentials. Cell 175, 57–70.e17. 10.1016/j.cell.2018.08.018. [PubMed: 30220455]

57. Kato S, Kaplan HS, Schrödel T, Skora S, Lindsay TH, Yemini E, Lockery S, and Zimmer M (2015). Global brain dynamics embed the motor command sequence of Caenorhabditis elegans. Cell 163, 656–669. 10.1016/j.cell.2015.09.034. [PubMed: 26478179]

58. Hallinen KM, Dempsey R, Scholz M, Yu X, Linder A, Randi F, Sharma AK, Shaevitz JW, and Leifer AM (2021). Decoding locomotion from population neural activity in moving C. elegans. eLife 10, e66135. 10.7554/eLife.66135. [PubMed: 34323218]

59. Amargós-Bosch M, Bortolozzi A, Puig MV, Serrats J, Adell A, Celada P, Toth M, Mengod G, and Artigas F (2004). Co-expression and in vivo interaction of serotonin1A and serotonin2A receptors in pyramidal neurons of prefrontal cortex. Cereb. Cortex N. Y. N 1991 14, 281–299. 10.1093/cercor/bhg128.

60. Pokala N, and Flavell SW (2022). Recording and Quantifying C. elegans Behavior. Methods Mol. Biol. Clifton NJ 2468, 357–373. 10.1007/978-1-0716-2181-3_20.

61. Cermak N, Yu SK, Clark R, Huang Y-C, Baskoylu SN, and Flavell SW (2020). Whole-organism behavioral profiling reveals a role for dopamine in state-dependent motor program coupling in C. elegans. eLife 9, e57093. 10.7554/eLife.57093. [PubMed: 32510332]

62. Mathis A, Mamidanna P, Cury KM, Abe T, Murthy VN, Mathis MW, and Bethge M (2018). DeepLabCut: markerless pose estimation of user-defined body parts with deep learning. Nat. Neurosci. 21, 1281–1289. 10.1038/s41593-018-0209-y. [PubMed: 30127430]

Highlights

- Extrasynaptic serotonin modulates foraging via six serotonin receptors
- Receptors mediate behavioral responses to serotonin with different in vivo kinetics
- Serotonin receptor expression patterns are mapped to the *C. elegans* connectome
- Brain-wide recordings with neuronal ID reveal serotonin-associated brain dynamics

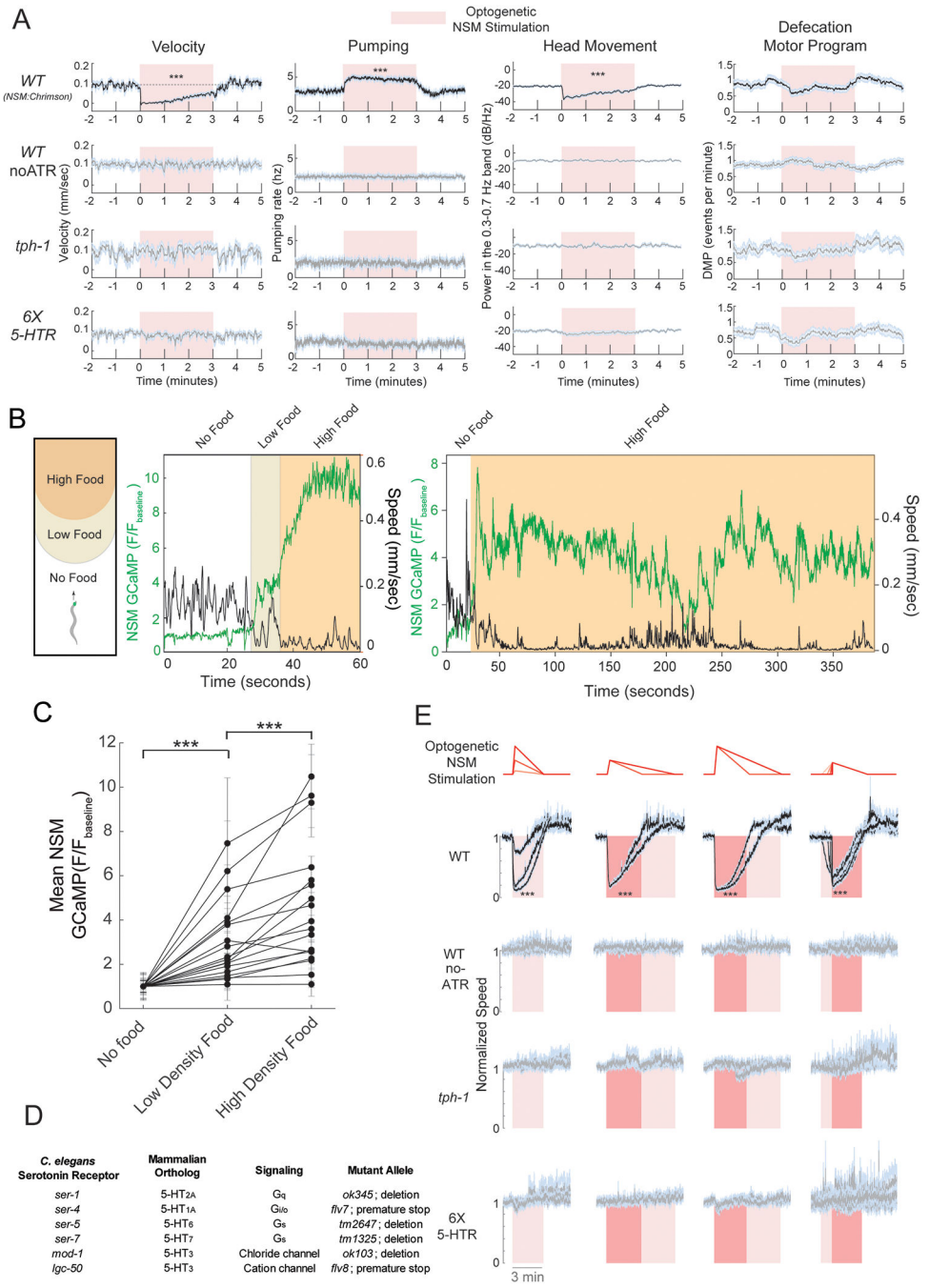

C. elegans Serotonin Receptor	Mammalian Ortholog	Signaling	Mutant Allele
ser-1	5-HT$_{2A}$	G_q	*ok345*; deletion
ser-4	5-HT$_{1A}$	$G_{i/o}$	*flv7*; premature stop
ser-5	5-HT$_6$	G_s	*tm2647*; deletion
ser-7	5-HT$_7$	G_s	*tm1325*; deletion
mod-1	5-HT$_3$	Chloride channel	*ok103*; deletion
lgc-50	5-HT$_3$	Cation channel	*flv8*; premature stop

Figure 1. The serotonergic neuron NSM provides an experimental platform for studying serotonin-induced behavioral changes

(A) Behavioral changes evoked by NSM::Chrimson activation. ***p<0.001, behavior change during lights-on, Bonferroni-corrected t-test. n=24–78 trials. Data are means ± standard error of the mean (SEM).

(B) Left: cartoon of assay. Right: Two example recordings of NSM (green) and animal speed (black). Shading indicates animal position in arena.

(C) Mean NSM GCaMP signal in each region of the arena. Data are means ± standard deviation. Each line is one animal. ***p<0.001, paired t-test. n=16 animals.

(D) *C. elegans* serotonin receptors and their properties.
(E) Changes in speed induced by NSM::Chrimson activation with the indicated waveforms of light (top, red). ***p<0.001, behavior change during lights-on, Bonferroni-corrected t-test. n=104–518 animals. Data are means of animal speed (normalized to pre-stimulus baseline speed) ± SEM.
See also Figure S1.

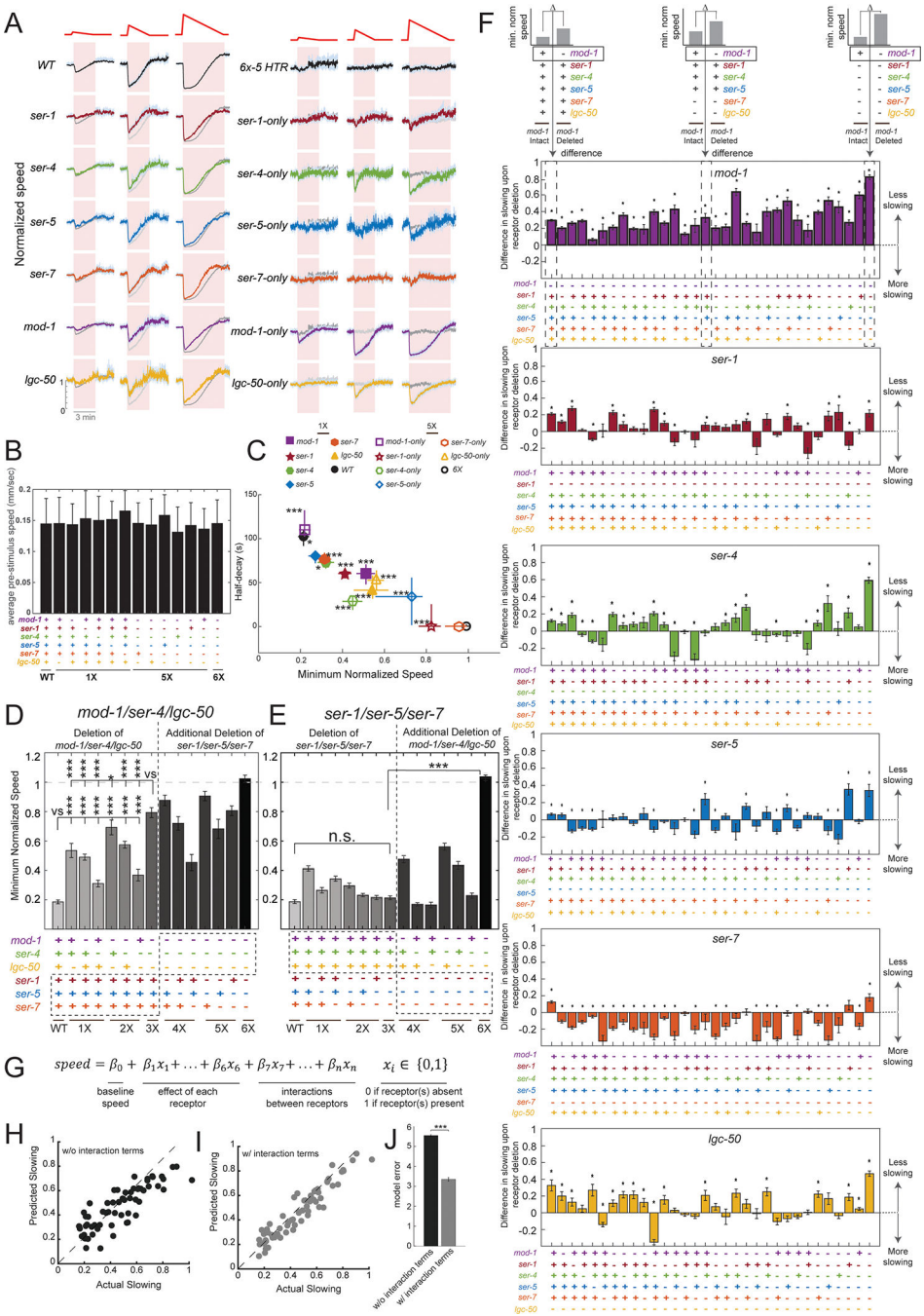

Figure 2. Six serotonin receptors interact to drive the locomotion changes elicited by NSM activation

(A) Speed changes induced by NSM::Chrimson activation. Gray traces in lower rows reproduce the trace from the top row. Data are means ± SEM.

(B) Baseline speeds of animals prior to NSM stimulation. n=45–496 animals. Data are means ± standard deviation.

(C) Quantification of speed traces for the medium intensity stimulus in (A). For single mutants, *p<0.05, ***p<0.001 versus WT for minimum speed and decay. For quintuple mutants, ***p<0.001 versus sextutple mutants for minimum speed, Bonferroni-corrected

empirical p-value that difference is non-zero. n=45–496 animals. Data are means ± 95% confidence interval (CI).

(D) Minimum normalized speed during medium intensity NSM stimulation. Pluses and minuses indicate genotype by indicating presence or absence (i.e. mutation) of each receptor. *p<0.05, ***p<0.001, empirical p-value that difference between distributions is non-zero. n=98–496 animals.

(E) Minimum normalized speed during NSM activation, displayed as in (D). ***p<0.001, empirical p-value that difference between distributions is non-zero. n=59–477 animals.

(F) Change in NSM-induced slowing caused by a given receptor's mutation, when other serotonin receptors are already mutated, shown for the medium intensity stimulus. Top graphic illustrates how y-axis values were calculated. Data are means ± SEM. *Benjamini-Hochberg FDR < 0.05. Average n=278 animals. See Methods for additional details.

(G) Equation used to predict NSM-induced slowing of animals based on serotonin receptor genotype.

(H-I) Model accuracy evaluated on the testing data from 5-fold crossvalidation without (H) and with (I) interaction terms included, as described in the text. Each dot is a genotype.

(J) Comparison of model performance. Data are the mean error ± standard deviations of five models from 5-fold crossvalidation. ***p<0.001, t-test.

See also Figure S2.

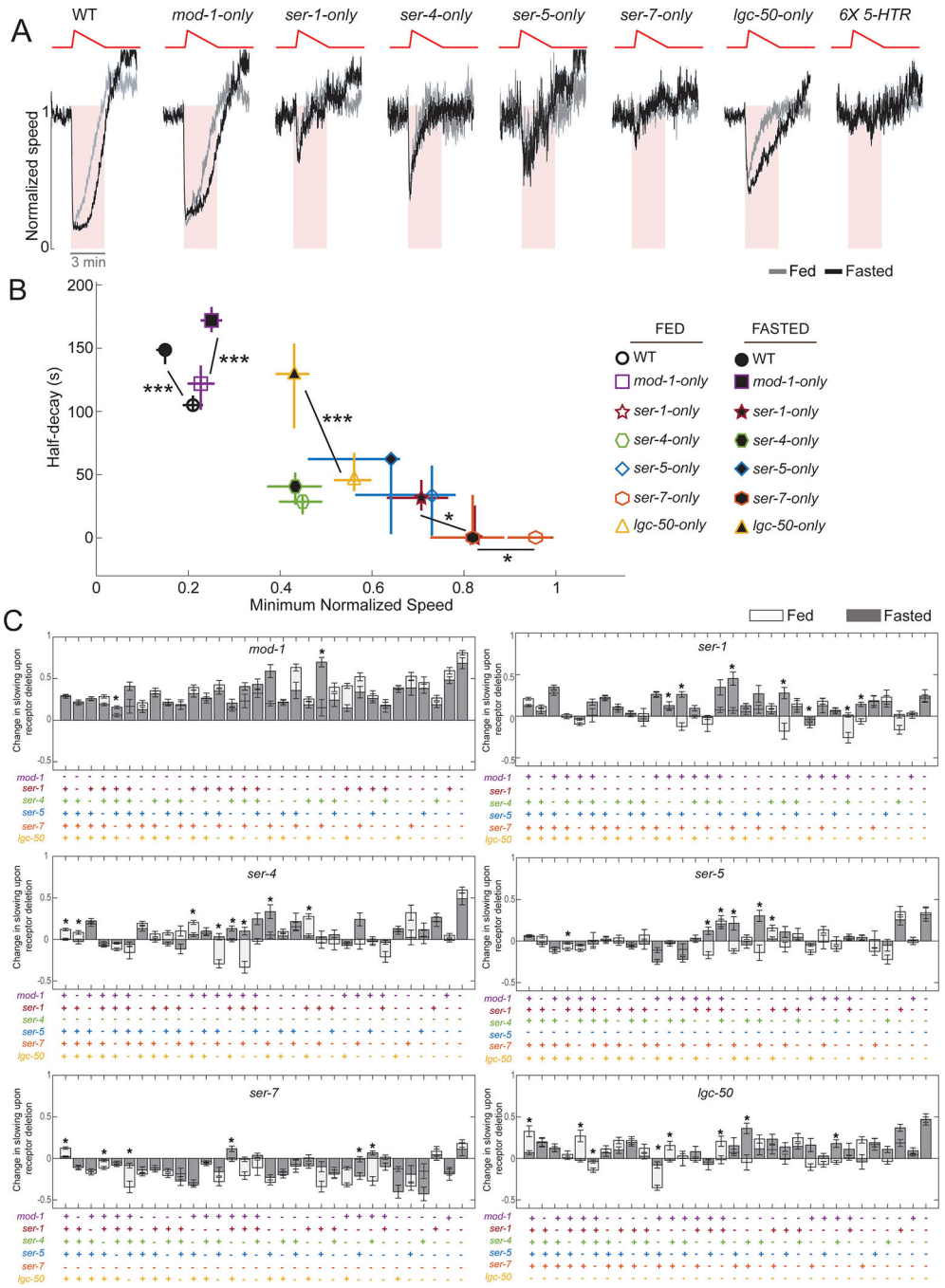

Figure 3. Satiety impacts how the serotonin receptors control locomotion

(A) Speed changes during NSM activation. Data are means ± SEM.

(B) Quantification of (B). N=44–495 animals. *p<0.05, ***p<0.001, slowing in fed versus fasted, Bonferroni-corrected empirical p-value that difference between distributions of either level or decay of slowing is non-zero.

(C) Change in NSM-induced slowing caused by receptor mutation, in different genetic backgrounds, displayed as in Fig. 2F. *p<0.05, Bonferroni-corrected empirical p-value, fed

versus fasted. See Methods for additional details. Average n=278 and 328 for fed and fasted, respectively. Data are means ± SEM.
See also Figure S3.

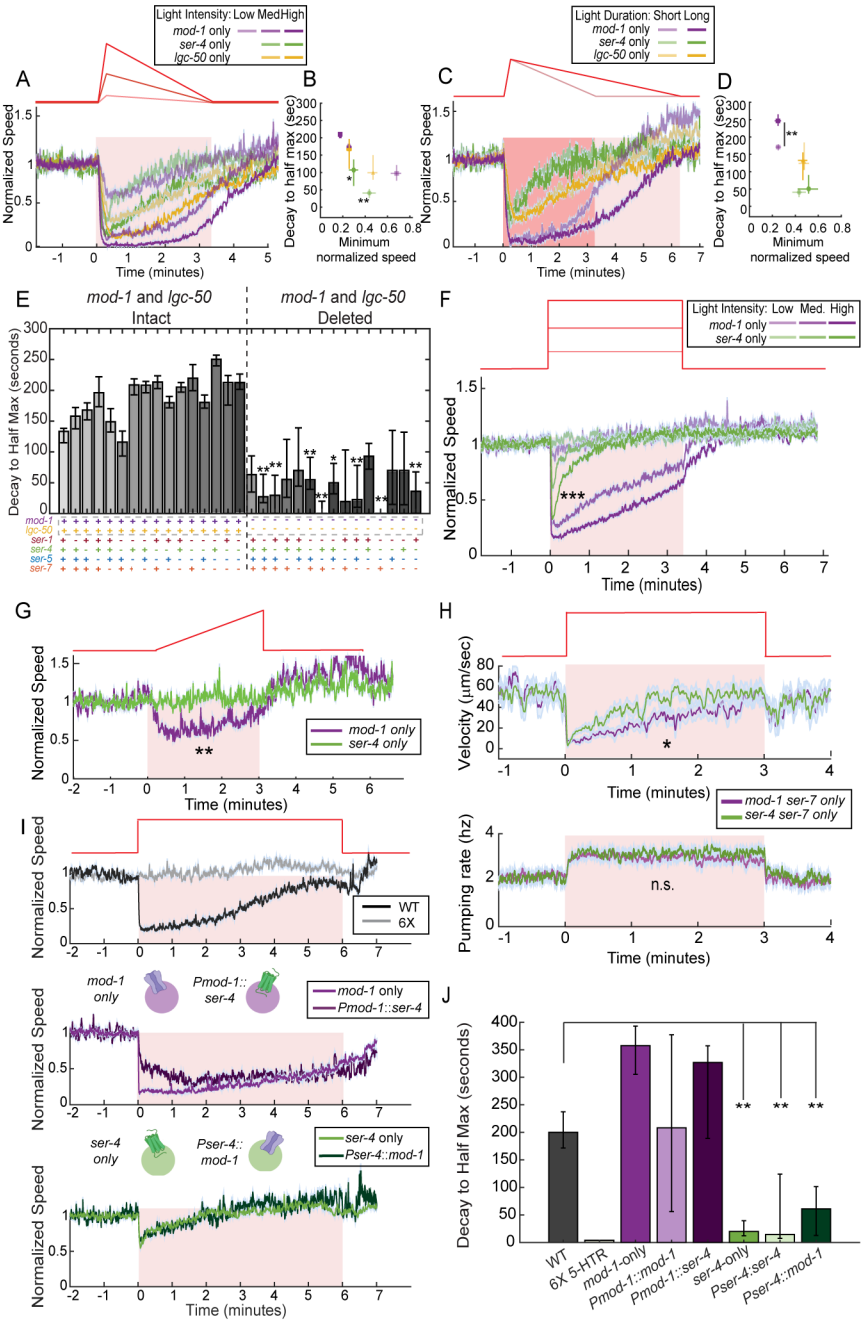

Figure 4. The *ser-4* and *mod-1* serotonin receptors mediate responses to different patterns of serotonin release, due to their distinct sites of expression

(A) Speed changes during NSM::Chrimson activation.

(B) Quantification of (A). **p<0.01, *ser-4*-only medium intensity stimulation versus all others; *p<0.05, *ser-4*-only high intensity stimulation versus *lgc-50*-only high intensity and *mod-1*-only medium and high intensity, Bonferroni-corrected empirical p-value that difference of decays is non-zero. n=116–495 animals.

(C) Speed changes during NSM::Chrimson activation.

(D) Quantification of (C). **p<0.01, medium- versus high-intensity stimulation, Bonferroni-corrected empirical p-value that difference of decays is non-zero. n=103–495 animals.
(E) Speed decay rates back to baseline after maximal slowing. *p<0.05, **p<0.01, WT versus indicated genotype, Bonferroni-corrected empirical p-value that difference is non-zero. Average n=284.
(F) Speed changes during NSM::Chrimson activation. ***p<0.001, max intensity *ser-4*-only condition versus medium-intensity *mod-1*-only condition since they are most closely matched for level of slowing, empirical p-value that difference of decays is non-zero. n=356–438 animals.
(G) Speed changes during NSM::Chrimson activation. **p<0.01, empirical p-value that difference in level of slowing is non-zero. n=177–466 animals.
(H) Velocity and feeding rate changes during NSM::Chrimson activation. *p<0.05, Bonferroni-corrected t-test of lights-on behavior. n.s., not significant. n=84–96 trials.
(I) Speed changes during NSM::Chrimson activation. Inset cartoons depict receptor swap transgenic lines.
(J) Quantification of (I). Decay back to baseline speed after maximal slowing. **p<0.01, WT vs. indicated genotypes, Bonferroni-corrected empirical p-value that difference between distributions is non-zero. n=47–306 animals.
For (A), (C), and (F-I): data are means ± SEM. For (B), (D-E), and (J): data are means ± 95% CI.
See also Figure S4.

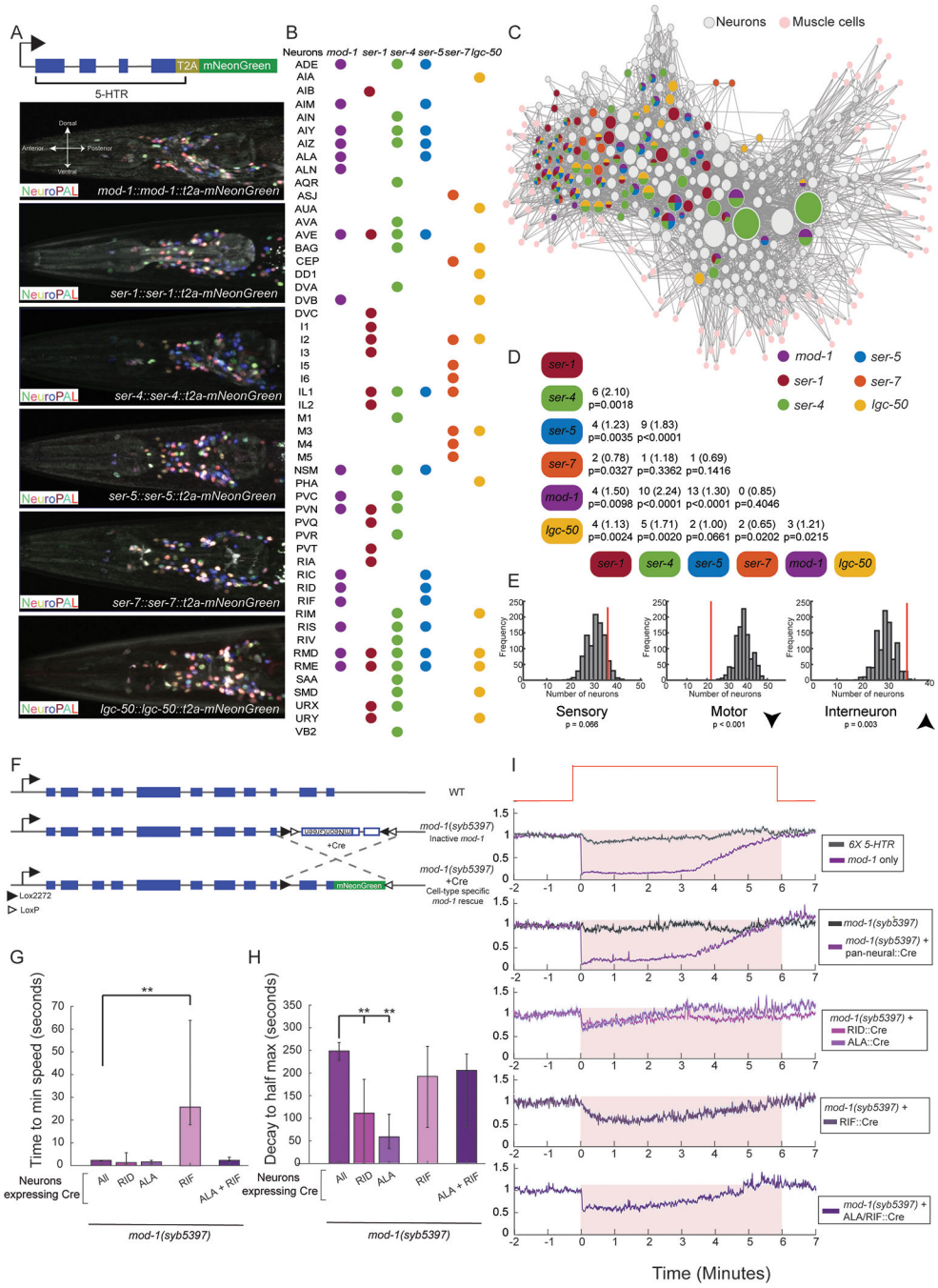

Figure 5. Mapping all sites of serotonin receptor expression across the *C. elegans* connectome

(A) Top: CRISPR/Cas9 editing strategy to introduce mNeonGreen reporter into native serotonin receptor genes. Below: Example images depicting mNeonGreen reporter expression for each receptor (white) and NeuroPAL labels (colors).

(B) A list of which serotonin receptor gene reporters were detected in which neuron classes. Dots indicate detected expression. Neurons without expression are not listed.

(C) *C. elegans* wiring diagram, with colors illustrating receptor expression. Adjacency of neurons indicates interconnected wiring. Node size is proportional to the number of synapses formed and received by the neuron.
(D) Overlap in receptor expression and, in parentheses, the number expected by chance. Multiple comparison-corrected p-value is from the permutation test (see Methods).
(E) Expression of serotonin receptors in sensory neurons, interneurons, and motor neurons. Red line indicates the actual number of receptors observed and the gray histogram indicates the chance levels from 1000 bootstraps. Multiple comparison-corrected p-value is from permutation test (see Methods).
(F) CRISPR/Cas9 gene editing was used to engineer a *mod-1* allele that is inactive (middle) until Cre expression inverts the exons back to their active orientation (bottom).
(G) Quantification of data in (I). Promoters: *Primb-1* (pan-neuronal), *Pflp-14* (RID), *Pver-3* (ALA), *Podr-2b* (RIF). **p<0.01, pan-neuronal Cre versus indicated line, Bonferroni-corrected empirical p-value that difference is non-zero. n=41–157 animals. Data are means ± 95% CI.
(H) Quantification of data in (I). **p<0.01, pan-neuronal Cre versus indicated line, Bonferroni-corrected empirical p-value that difference is non-zero. n=41–157 animals. Data are means ± 95% CI.
(I) Changes in animal speed during NSM::Chrimson activation. Data are means ± SEM. See also Figure S5.

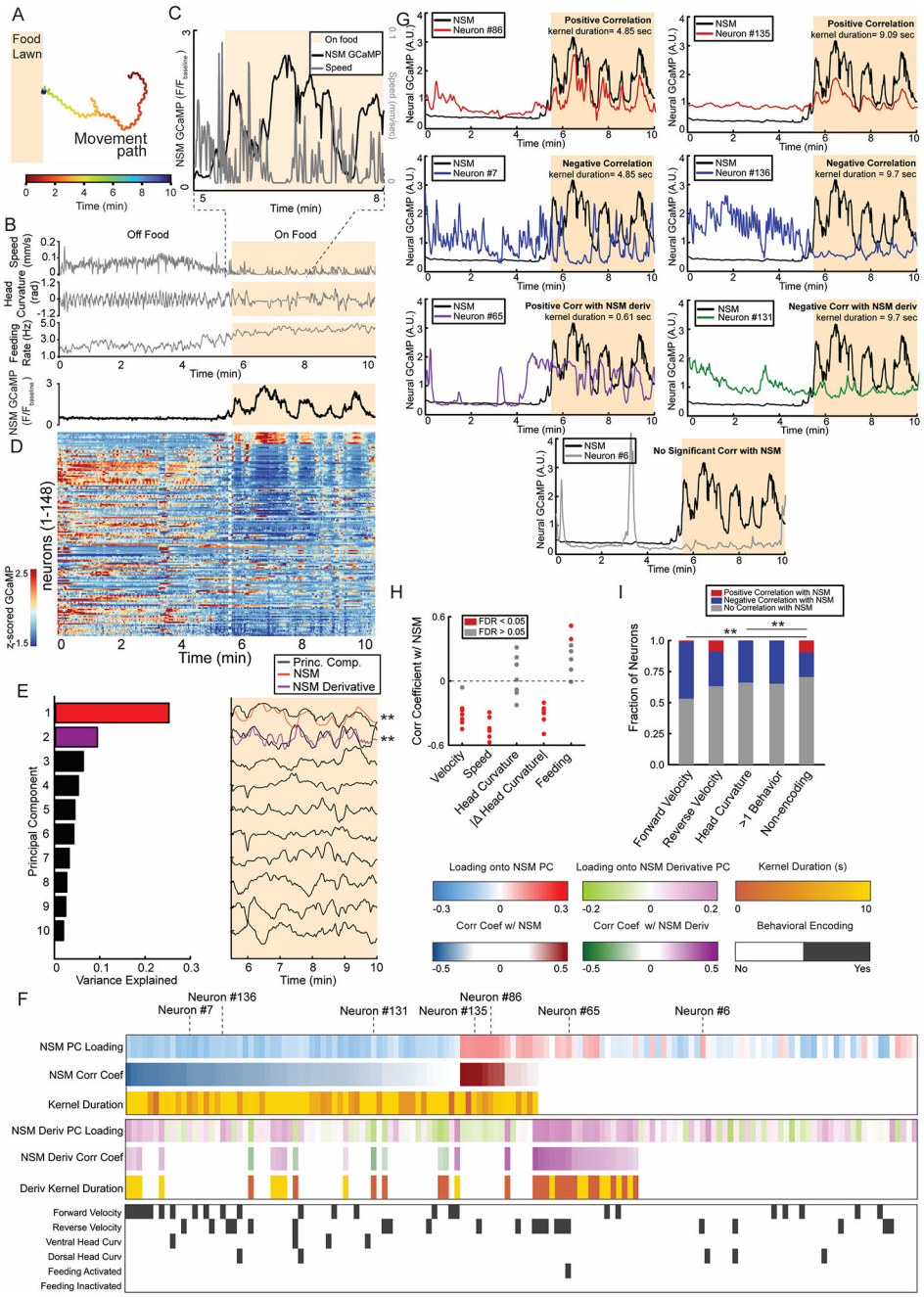

Figure 6. NSM activity is associated with widespread changes in brain-wide dynamics in freely-moving animals

(A) Example animal movement path during a freely-moving brain-wide calcium recording.

(B) Example behavioral and NSM GCaMP data from the freely-moving brain-wide recording in (A). Beige background indicates the on-food time epoch.

(C) Zoomed detail of (B).

(D) Heatmap depicting GCaMP data from 148 neurons.

(E) PCA analysis of an example animal, from the on-food time epoch. Left: variance explained by each PC. Right: each PC over time. PC1 is correlated to NSM; PC2 is

correlated to the derivative of NSM (**p<0.01, Benjamini-Hochberg-corrected shuffle test, see Methods). NSM correlates to one of the top 3 PCs in all animals, and its derivative correlates to one of the top PCs in most animals.

(F) An analysis of all neurons in an example animal. Each neuron is a column and the rows show:

(1) NSM PC loading: factor loadings for PC1.

(2) NSM Corr Coef: correlation coefficient of the neuron with kernel-convolved NSM (see text and Methods). Values are only shown if correlation is significant (FDR<0.1, Benjamini-Hochberg-corrected shuffle test).

(3) Duration of the kernel from (2).

(4) NSM Deriv PC Loading: factor loadings for PC2.

(5) NSM Deriv Corr Coef: the correlation coefficient of the neuron with its optimal differentiator-kernel-convolved NSM, shown as in (2).

(6) Duration of the kernel from (5).

(7) How each neuron encoded behavior in the off-food time epoch (see Methods). Gray bar indicates significant encoding.

(G) Example neurons from the recording in (A-F), shown alongside NSM activity. Red neurons have positive correlation with NSM; blue ones have negative correlation; purple and green neurons are correlated with NSM derivative; gray neuron has no correlation to NSM.

(H) The correlation of NSM with different behaviors. Each dot depicts a different dataset. Red dots indicate significance, FDR<0.05, Benjamini-Hochberg-corrected shuffle test.

(I) How neurons that encode different motor programs off-food are associated with NSM activity on-food. **p<0.01, Benjamini-Hochberg-corrected Chi-squared test.

See also Figure S6.

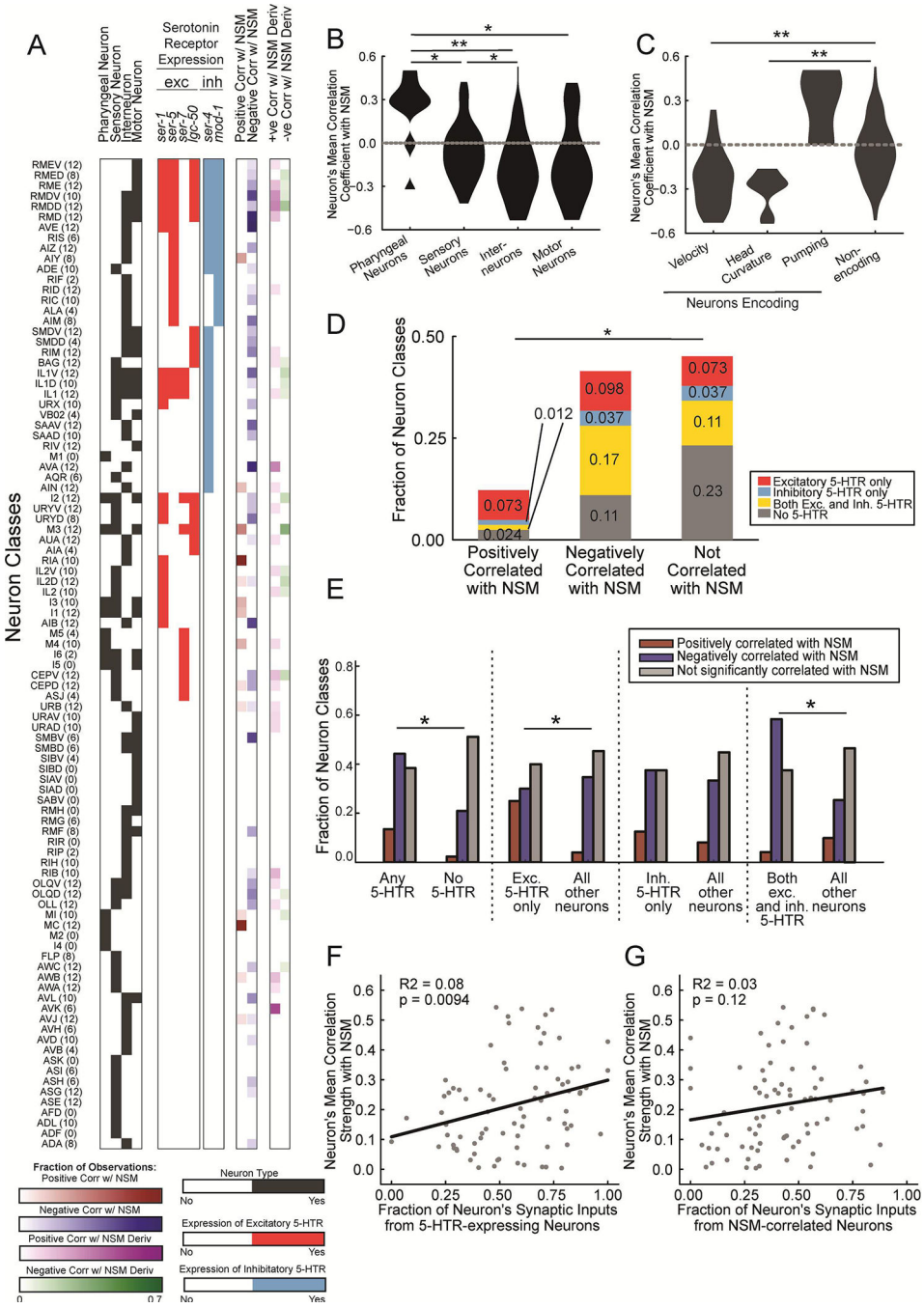

Figure 7. How neurons in the *C. elegans* brain are functionally coupled to NSM, based on serotonin receptor expression, connectivity, and behavioral functions

(A) A list of *C. elegans* neuron classes, with information about the neurons provided in the columns (parentheses indicates number of recordings for neuron):

(1) Columns 1–4: Type of neuron.

(2) Columns 5–10: Serotonin receptor expression pattern (excitatory receptors are red; inhibitory receptors are blue).

(3) Columns 11–12: Fraction of times neuron was correlated with NSM.

(4) Columns 13–14: Fraction of times neuron was correlated with NSM derivative.

(B-C) Mean correlation of the *C. elegans* neuron classes with NSM, split by neuron category (B) or how neurons encode behavior (C). *p<0.05, **p<0.01, Benjamini-Hochberg-corrected Generalized Wilcoxon test.

(D-E) The relationship between serotonin receptor expression and how neuron is correlated with NSM. Neuron classes were classified as being correlated with NSM if they achieved significance in >10% of recordings. *p<0.05, Benjamini-Hochberg-corrected Chi-square test.

(F-G) Relationship between each neuron class' correlation with NSM and its presynaptic partners' serotonin receptor expression (F) or correlations to NSM (G). Inset shows variance explained and p-value of line of best fit.

See also Figure S7.

KEY RESOURCES TABLE

REAGENT or RESOURCE	SOURCE	IDENTIFIER
Antibodies		
Bacterial and Virus Strains		
E. coli: Strain OP50	*Caenorhabditis* Genetics Center	OP50
Chemicals, Peptides, and Recombinant Proteins		
Critical Commercial Assays		
Deposited Data		
Original code and data related to neural activity and behavior	This paper	http://doi.org/10.5281/zenodo.7830052 https://github.com/flavell-lab/NSM_5HTR_analysis/tree/publication_withdata
Experimental Models: Organisms/Strains		
C. elegans: Wild-type Bristol N2	*Caenorhabditis* Genetics Center	N2
C. elegans: lgc-50(*syb4186*) [T2A-mNeonGreen insertion]	This Paper	PHX4186
C. elegans: ser-1(*syb1805*) [T2A-mNeonGreen insertion]	This Paper	PHX1805
C. elegans: ser-4(*syb4754*) [T2A-mNeonGreen insertion]	This Paper	PHX4754
C. elegans: ser-5(*syb4159*) [T2A-mNeonGreen insertion]	This Paper	PHX4159
C. elegans: ser-7(*syb1941*) [T2A-mNeonGreen insertion]	This Paper	PHX1941
C. elegans: mod-1(*syb1841*) [T2A-mNeonGreen insertion]	This Paper	PHX1841
C. elegans: flvIs2[tph-1(short)::Chrimson, elt-2::mCherry]; flvEx146[Pdel-7::GCaMP6m, myo2::mCherry]	This Paper	SWF828
C. elegans: flvEx146[Pdel-7::GCaMP6m, myo2::mCherry],	This Paper	SWF849
C. elegans: flvIs2[tph-1(short)::Chrimson, elt-2::mCherry]	This Paper	SWF 117
C. elegans: mod-1(ok103); ser-1(ok345); ser-4(flv7); ser-5(tm2647); ser-7(tm1325); lgc-50(flv8); flvIs2[Ptph-1(short)::Chrimson, Pelt-2::mCherry]	This Paper	SWF380
C. elegans: mod-1(ok103); flvIs2[Ptph-1(short)::Chrimson, Pelt-2::mCherry]	This Paper	SWF 142
C. elegans: ser-1(ok345); flvIs2[Ptph-1(short)::Chrimson, Pelt-2::mCherry]	This Paper	SWF 154
C. elegans: ser-4(flv7); flvIs2[tph-1(short)::Chrimson, elt-2::mCherry]	This Paper	SWF193
C. elegans: ser-5(tm2647); flvIs2[Ptph-1(short)::Chrimson, Pelt-2::mCherry]	This Paper	SWF150
C. elegans: ser-7(tm1325); flvIs2[Ptph-1(short)::Chrimson, Pelt-2::mCherry]	This Paper	SWF155
C. elegans: lgc-50(flv8); flvIs2[tph-1(short)::Chrimson, elt-2::mCherry]	This Paper	SWF912
C. elegans: ser-1(ok345); ser-4(flv7); flvIs2[Ptph-1(short)::Chrimson, Pelt-2::mCherry]	This Paper	SWF290
C. elegans: ser-1(ok345); ser-5(tm2647); flvIs2[Ptph-1(short)::Chrimson, Pelt-2::mCherry]	This Paper	SWF280
C. elegans: ser-1(ok345); ser-7(tm1325); flvIs2[Ptph-1(short)::Chrimson, Pelt-2::mCherry]	This Paper	SWF281

REAGENT or RESOURCE	SOURCE	IDENTIFIER
C. elegans: mod-1(ok103); ser-1(ok345); flvIs2[tph-1(short)::Chrimson, elt-2::mCherry]	This Paper	SWF173
C. elegans: ser-1(ok345); lgc-50(flv8); flvIs2[Ptph-1(short)::Chrimson, Pelt-2::mCherry]	This Paper	SWF449
C. elegans: ser-4(flv7); ser-5(tm2647); flvIs2[Ptph-1(short)::Chrimson, Pelt-2::mCherry]	This Paper	SWF291
C. elegans: ser-4(flv7); ser-7(tm1325); flvIs2[Ptph-1(short)::Chrimson, Pelt-2::mCherry]	This Paper	SWF292
C. elegans: mod-1(ok103); ser-4(flv7); flvIs2[tph-1(short)::Chrimson, elt-2::mCherry]	This Paper	SWF250
C. elegans: ser-4(flv7); lgc-50(flv8); flvIs2[Ptph-1(short)::Chrimson, Pelt-2::mCherry]	This Paper	SWF426
C. elegans: ser-5(tm2647); ser-7(tm1325); flvIs2[Ptph-1(short)::Chrimson, Pelt-2::mCherry]	This Paper	SWF282
C. elegans: mod-1(ok103); ser-5(tm2647); flvIs2[tph-1(short)::Chrimson, elt-2::mCherry]	This Paper	SWF 171
C. elegans: ser-5(tm2647); lgc-50(flv8); flvIs2[Ptph-1(short)::Chrimson, Pelt-2::mCherry]	This Paper	SWF450
C. elegans: mod-1(ok103); ser-7(tm1325); flvIs2[tph-1(short)::Chrimson, elt-2::mCherry]	This Paper	SWF172
C. elegans: ser-7(tm1325); lgc-50(flv8); flvIs2[Ptph-1(short)::Chrimson, Pelt-2::mCherry]	This Paper	SWF475
C. elegans: mod-1(ok103); lgc-50(flv8); flvIs2[tph-1(short)::Chrimson, elt-2::mCherry]	This Paper	SWF900
C. elegans: ser-1(ok345); ser-4 (flv7); ser-5(tm2647); flvIs2[Ptph-1(short)::Chrimson, Pelt-2::mCherry]	This Paper	SWF294
C. elegans: ser-1(ok345); ser-4(flv7); ser-7(tm1325); flvIs2[Ptph-1(short)::Chrimson, Pelt-2::mCherry]	This Paper	SWF293
C. elegans: mod-1 (ok103); ser-1 (ok345); ser-4 (flv7); flvIs2[Ptph-1(short)::Chrimson, Pelt-2::mCherry]	This Paper	SWF298
C. elegans: ser-1(ok345); ser-4(flv7); lgc-50(flv8); flvIs2[Ptph-1(short)::Chrimson, Pelt-2::mCherry]	This Paper	SWF431
C. elegans: ser-1(ok345); ser-5(tm2647); ser-7(tm1325); flvIs2[Ptph-1(short)::Chrimson, Pelt-2::mCherry]	This Paper	SWF279
C. elegans: mod-1(ok103) V; ser-1(ok345); ser-5(tm2647); flvIs2[Ptph-1(short)::Chrimson, Pelt-2::mCherry]	This Paper	SWF276
C. elegans: ser-1(ok345); ser-5(tm2647); lgc-50(flv8); flvIs2[Ptph-1(short)::Chrimson, Pelt-2::mCherry]	This Paper	SWF901
C. elegans: mod-1(ok103) V; ser-1(ok345); ser-7(tm1325); flvIs2[Ptph-1(short)::Chrimson, Pelt-2::mCherry]	This Paper	SWF277
C. elegans: ser-1(ok345); ser-7(tm1325); lgc-50(flv8); flvIs2[Ptph-1(short)::Chrimson, Pelt-2::mCherry]	This Paper	SWF902
C. elegans: mod-1(ok103) V; ser-1 (ok345); lgc-50(flv8); flvIs2[Ptph-1(short)::Chrimson, Pelt-2::mCherry]	This Paper	SWF903
C. elegans: ser-4(flv7); ser-5(tm2647); ser-7(tm1325); flvIs2[Ptph-1(short)::Chrimson, Pelt-2::mCherry]	This Paper	SWF295
C. elegans: mod-1(ok103); ser-4(flv7); ser-5(tm2647); flvIs2[Ptph-1(short)::Chrimson, Pelt-2::mCherry]	This Paper	SWF296
C. elegans: ser-4(flv7); ser-5(tm2647); lgc-50(flv8); flvIs2[Ptph-1(short)::Chrimson, Pelt-2::mCherry]	This Paper	SWF485

REAGENT or RESOURCE	SOURCE	IDENTIFIER
C. elegans: mod-1(ok103); ser-4(flv7); ser-7(tm1325); flvIs2[Ptph-1(short)::Chrimson, Pelt-2::mCherry]	This Paper	SWF297
C. elegans: ser-4(flv7); ser-7(tm1325); lgc-50(flv8); flvIs2[Ptph-1(short)::Chrimson, Pelt-2::mCherry]	This Paper	SWF423
C. elegans: mod-1(ok103); ser-4(flv7); lgc-50(flv8); flvIs2[Ptph-1 (short)::Chrimson, Pelt-2::mCherry]	This Paper	SWF419
C. elegans: mod-1(ok103) V; ser-5(tm2647); ser-7(tm1325); flvIs2[Ptph-1(short)::Chrimson, Pelt-2::mCherry]	This Paper	SWF278
C. elegans: ser-5(tm2647); ser-7(tm1325); lgc-50(flv8); flvIs2[Ptph-1(short)::Chrimson, Pelt-2::mCherry]	This Paper	SWF463
C. elegans: mod-1(ok103) V; ser-5(tm2647); lgc-50(flv8); flvIs2[Ptph-1(short)::Chrimson, Pelt-2::mCherry]	This Paper	SWF904
C. elegans: mod-1(ok103) V; ser-7(tm1325); lgc-50(flv8); flvIs2[Ptph-1(short)::Chrimson, Pelt-2::mCherry]	This Paper	SWF905
C. elegans: ser-1(ok345); ser-4(flv7); ser-5(tm2647); ser-7(tm1325); flvIs2[Ptph-1(short)::Chrimson, Pelt-2::mCherry]	This Paper	SWF303
C. elegans: mod-1(ok103); ser-1(ok345); ser-4(flv7); ser-5(tm2647); flvIs2[Ptph-1(short)::Chrimson, Pelt-2::mCherry]	This Paper	SWF299
C. elegans: ser-1(ok345); ser-4(flv7); ser-5(tm2647); lgc-50(flv8); flvIs2[Ptph-1(short)::Chrimson, Pelt-2::mCherry]	This Paper	SWF422
C. elegans: mod-1 (ok103); ser-1 (ok345); ser-4 (flv7); ser-7 (tm1325); flvIs2[Ptph-1(short)::Chrimson, Pelt-2::mCherry]	This Paper	SWF300
C. elegans: mod-1(ok103); ser-1(ok345); ser-4(flv7); lgc-50(flv8); flvIs2[Ptph-1(short)::Chrimson, Pelt-2::mCherry]	This Paper	SWF906
C. elegans: mod-1(ok103) V; ser-1(ok345); ser-5(tm2647); ser-7(tm1325); flvIs2[Ptph-1(short)::Chrimson, Pelt-2::mCherry]	This Paper	SWF275
C. elegans: ser-1(ok345); ser-5(tm2647); ser-7(tm1325); lgc-50(flv8); flvIs2[Ptph-1(short)::Chrimson, Pelt-2::mCherry]	This Paper	SWF907
C. elegans: mod-1(ok103); ser-1(ok345); ser-5(tm2647); lgc-50(flv8); flvIs2[Ptph-1(short)::Chrimson, Pelt-2::mCherry]	This Paper	SWF458
C. elegans: mod-1(ok103); ser-1(ok345); ser-7(tm1325); lgc-50(flv8); flvIs2[Ptph-1(short)::Chrimson, Pelt-2::mCherry]	This Paper	SWF908
C. elegans: mod-1(ok103); ser-4(flv7); ser-5(tm2647); ser-7(tm1325); flvIs2[Ptph-1(short)::Chrimson, Pelt-2::mCherry]	This Paper	SWF301
C. elegans: ser-4(flv7); ser-5(tm2647); ser-7(tm1325); lgc-50(flv8); flvIs2[Ptph-1(short)::Chrimson, Pelt-2::mCherry]	This Paper	SWF421
C. elegans: ser-1(ok345); ser-4(flv7); ser-7(tm1325); lgc-50(flv8); flvIs2[Ptph-1(short)::Chrimson, Pelt-2::mCherry]	This Paper	SWF427
C. elegans: mod-1(ok103); ser-4(flv7); ser-5(tm2647); lgc-50(flv8); flvIs2[Ptph-1(short)::Chrimson, Pelt-2::mCherry]	This Paper	SWF425
C. elegans: mod-1(ok103); ser-4(flv7); ser-7(tm1325); lgc-50(flv8); flvIs2[Ptph-1(short)::Chrimson, Pelt-2::mCherry]	This Paper	SWF909
C. elegans: mod-1(ok103); ser-5(tm2647); ser-7(tm1325); lgc-50(flv8); flvIs2[Ptph-1(short)::Chrimson, Pelt-2::mCherry]	This Paper	SWF910
C. elegans: mod-1(ok103); ser-4(flv7); ser-5(tm2647); ser-7(tm1325); lgc-50(flv8); flvIs2[Ptph-1(short)::Chrimson, Pelt-2::mCherry]	This Paper	SWF911
C. elegans: mod-1(ok103); ser-1(ok345); ser-5(tm2647); ser-7(tm1325); lgc-50(flv8); flvIs2[Ptph-1(short)::Chrimson, Pelt-2::mCherry]	This Paper	SWF469
C. elegans: mod-1(ok103); ser-1(ok345); ser-4(flv7); ser-7(tm1325); lgc-50(flv8); flvIs2[Ptph-1(short)::Chrimson, Pelt-2::mCherry]	This Paper	SWF420

REAGENT or RESOURCE	SOURCE	IDENTIFIER
C. elegans: mod-1(ok103); ser-1(ok345); ser-4(flv7); ser-5(tm2647); lgc-50(flv8); flvIs2[Ptph-1(short)::Chrimson, Pelt-2::mCherry]	This Paper	SWF424
C. elegans: ser-1(ok345); ser-4(flv7); ser-5(tm2647); ser-7(tm1325); lgc-50(flv8); flvIs2[Ptph-1(short)::Chrimson, Pelt-2::mCherry]	This Paper	SWF800
C. elegans: mod-1(ok103); ser-1(ok345); ser-4(flv7); ser-5(tm2647); ser-7(tm1325); flvIs2[Ptph-1(short)::Chrimson, Pelt-2::mCherry]	This Paper	SWF302
C. elegans: mod-1(ok103); ser-1(ok345); ser-4(flv7); ser-5(tm2647); ser-7(tm1325); lgc-50(flv8); flvIs2; flvEx336[Pser4::mod1, myo3::mCherry]	This Paper	SWF740
C. elegans: mod-1(ok103); ser-1(ok345); ser-4(flv7); ser-5(tm2647); ser-7(tm1325); lgc-50(flv8); flvIs2; flvEx333[Pmod1::ser4, myo3::mCherry]	This Paper	SWF737
C. elegans: mod-1(ok103); ser-1(ok345); ser-4(flv7); ser-5(tm2647); ser-7(tm1325); lgc-50(flv8); flvIs2; flvEx314[Pser4::ser4, myo2::mCherry]	This Paper	SWF709
C. elegans: mod-1(ok103); ser-1(ok345); ser-4(flv7); ser-5(tm2647); ser-7(tm1325); lgc-50(flv8); flvIs2; flvEx3[Pmod1::mod1, myo2::mCherry]	This Paper	SWF713
C. elegans: mod-1(syb5397)	This Paper	PHX5397
C. elegans: mod-1(syb5397); flvEx331[rimb-1::nCre, myo3::mCherry]	This Paper	SWF735
C. elegans: mod-1(syb5397); flvEx415[flp-14::nCre, elt2::mCherry]	This Paper	SWF913
C. elegans: mod-1(syb5397); flvEx395[ver-3::nCre, myo3::mCherry]	This Paper	SWF836
C. elegans: mod-1(syb5397); flvEx411[odr-2b::nCre, elt2::mCherry]	This Paper	SWF871
C. elegans: mod-1(syb5397); flvEx384[odr-2b/ver-3::nCre, myo3::mCherry]	This Paper	SWF821
C. elegans: flvIs17[rimb-1::NLS-GCaMP7F, gcy-28.d::NLS-tag-RFPt, ceh-36:NLS-tag-RFPt, inx-1::tag-RFPt, mod-1::tag-RFPt, tph-1(short)::NLS-tag-RFPt, gcy-5::NLS-tag-RFPt, gcy-7::NLS-tag-RFPt]; flvIs18[rimb-1::NLS-mNeptune2.5]; lite-1(ce314); gur-3(ok2245)	This Paper	SWF415
C. elegans: flvIs17; otIs670 [low-brightness NeuroPAL]; lite-1(ce314); gur-3(ok2245)	This Paper	SWF702
Software and Algorithms		
MATLAB (2021)	Mathworks	https://www.mathworks.com
Streampix (v7.0)	Norpix	https://www.norpix.com
GraphPad Prism (v9)	Dotmatics	https://www.graphpad.com
Adobe Illustrator	Adobe	https://www.adobe.com
Dropbox	Dropbox	https://www.dropbox.com
Other		
SP-20000M-USB3 CMOS camera	JAI	N/A
Micro-NIKKOR 55mm f/2.8 lens	Nikon	N/A
10x25 White Panel LED backlight, 24VDC	Metaphase Technologies	Cat#MS-BL10X25-W-24-ILD-PS
Precision LED Spot Light, 625nm, 40W, Type H	Mightex	Cat#BLS-PLS-0625–030-40-S
BioLED Light Source Control Module	Mightex	Cat#BLS-13000–1